JOURNAL OF GUIDANCE, CONTROL, AND DYNAMICS
Vol. 35, No. 1, January–February 2012

Modeling and Direct Adaptive Control of a Flexible-Joint Manipulator

Steve Ulrich* and Jurek Z. Sasiadek†
Carleton University, Ottawa, Ontario K1S 5B6, Canada
and
Itzhak Barkana‡
Barkana Consulting, 47209 Ramat-Hasharon, Israel

DOI: 10.2514/1.54083

This paper addresses the problem of adaptive trajectory control of space manipulators that exhibit elastic vibrations in their joints and that are subject to parametric uncertainties and modeling errors. First, it presents a comprehensive study of rigid and linear flexible-joint stiffness models, to propose a dynamic formulation that includes nonlinear effects such as soft-windup and time-varying joint stiffness. Second, it develops an adaptive composite control scheme for tracking the end effector of a two-link flexible-joint manipulator. The control scheme consists of a direct model reference adaptive system designed to stabilize the rigid dynamics and a linear correction term to improve damping of vibrations at the joints. Numerical simulations compare the performance of the adaptive controller with its nonadaptive version in the context of a 12.6 × 12.6 m square trajectory tracking. Results obtained with the adaptive control strategy show an increased robustness to modeling errors and uncertainties in joint stiffness coefficients, and greatly improved tracking performance, compared with the nonadaptive strategy.

I. Introduction

STRUCTURAL flexibility of robot manipulators in space applications is a well-known problem, and various control strategies have been proposed in the literature to minimize the resulting vibrations [1–8]. In addition to link flexibility, joint flexibility is a major detrimental characteristic of large manipulators [9]. In fact, joint flexibility is often considered more important than link flexibility, at least in the operational range of space robots [10]. Although current space robots equipped with planetary gear trains, such as the Space Station Remote Manipulator, can exhibit considerable joint elasticity effects [11,12], these flexible behaviors are particularly important in lightweight manipulators equipped with harmonic drives [13], such as the DLR Lightweight Robot III. Harmonic drive joint mechanisms are becoming increasingly popular for use in space applications, due to their low weight, compactness, high torque capability, wide operating temperature range, and reliable repeatability. However, the flexibility effects of this type of gear mechanism in the joints of robotic manipulators are significant enough to make real-time operation challenging, particularly when accurate end-effector positioning is required [14]. Neglecting joint elasticity effects in control system design can also lead to instability [15]. The impacts of joint flexibility on the control system performance of space robotic manipulators were highlighted by Cetinkunt and Book [16]. In addition, control schemes based on rigid models of robots have limited or unacceptable applicability to practical situations. In particular, since flexible-joint dynamics model does not have an independent control input for each degree of freedom (DOF), most control algorithms designed for rigid-joint robots do not extend to the flexible-joint case, as explained by Ghorbel et al. [17]. Sasiadek [18] discusses how, elastic vibration of the joints, coupled with their large rotations and nonlinear dynamics, can also induce structural flexibility of the links.

This paper considers the trajectory-tracking control problem associated with flexible-joint manipulators in the presence of parametric uncertainties and modeling errors. Most of the preliminary studies of this problem are based on the singular perturbation theory [19], under which a flexible-joint robot exhibits a two-scale behavior. Using this theory, Spong [20,21], Ghorbel et al. [17] and Chang and Daniel [22] developed adaptive singular perturbation-based (SPB) controllers (also referred to as *adaptive composite controllers*) consisting of a slow adaptive control term designed on the basis of a rigid robot model and a fast control designed to dampen the elastic oscillations at the joints. However, the controllers proposed in these early studies were only applicable to manipulators with weak joint flexibility effects. Ott et al. [23] verified the well-known Slotine–Li adaptive composite controller experimentally, and though good tracking results are achieved, the proposed strategy relies mainly on joint torque measurements, which implies the use of additional sensors. An adaptive composite controller for a flexible-joint robot with uncertain parameters and constrained motion was presented by Huang et al. [24]. Though their tracking results were also good, the controller relies mainly on force feedback measurements. Fuzzy and neural network adaptive composite control laws have also been proposed for flexible-joint manipulators. Subudhi and Morris [25] developed an approach in which a neural network replaces the inverse dynamics control for the slow dynamics in order to cope with the model uncertainties. Cao and de Silva [26] applied neural-network-based adaptive composite control to a flexible manipulator, which included both revolute and deployable links.

These existing adaptive composite control methodologies cope with parametric uncertainties by identifying the unknown robot parameters used explicitly in their control algorithm. This approach is referred to as *indirect adaptive control*. For example, [26] uses neural networks to approximate the unknown manipulator's inertia and Coriolis matrices used in their control law. An adverse consequence of such identification procedures is the increased computational burden associated with real-time computation of unknown parameters. This drawback could rule out the use of such adaptive

Presented as Paper 2010-7844 at the AIAA Guidance, Navigation, and Control Conference, Toronto, Ontario, Canada, 2–5 August 2010; received 23 February 2011; revision received 10 May 2011; accepted for publication 11 May 2011.

*Ph.D. Candidate, Department of Mechanical and Aerospace Engineering, 1125 Colonel By Drive. Member AIAA.
†Professor, Department of Mechanical and Aerospace Engineering, 1125 Colonel By Drive. Associate Fellow AIAA.
‡President, 11 Hashomer Street. Associate Fellow AIAA.

controllers for space operations, where available computational resources are limited.

The main original contribution of this paper is the design of a *direct adaptive controller* for flexible-joint robots using the modified simple adaptive control (MSAC) technique [27], which is a technique derived upon the simple adaptive control (SAC) methodology [28]. Unlike existing adaptive controllers, the proposed design is an output feedback approach that does not require identification of unknown parameters or mathematical models of the system to be controlled. Specifically, the adaptive controller design proposed in this paper is based on the model reference adaptive control (MRAC) approach and deals with modeling errors and parameter uncertainties by time-varying the control gains using the MSAC law, in order to reduce the errors between an ideal model and the actual robot system.

Another deficiency of existing adaptive composite control schemes for flexible-joint manipulators is that they have been validated in numerical simulations using the classic Spong model [29]. Considered the centerpiece of nearly all work in the area of flexible-joint control, this basic dynamics formulation assumes that each joint is modeled as a linear torsional spring of constant stiffness. However, experimental studies [30–35] have revealed that joint mechanisms are far more complex than linear springs and they exhibit highly nonlinear effects. Therefore, in order to better capture nonlinear effects observed in experiments, a comprehensive dynamics model that simultaneously considers friction, nonlinear stiffness, soft-windup, and inertial cross-coupling is proposed in this paper. Both models will be used in numerical simulations to validate the performance of the adaptive controller in the context of a 12.6×12.6 m square trajectory tracking by a two-link manipulator.

This paper is organized as follows: Section II presents the derivation of a nonlinear joint model that includes the effects of friction, soft-windup, nonlinear stiffness, and inertial coupling. Section III reviews the SAC and MSAC control theories under which the direct adaptive composite controller is designed. In Sec. IV, the flexible-joint direct adaptive control design is presented, and key technical issues are examined, including elastic vibration damping and control gain adaptation laws. Section V consists of the stability analysis of the proposed direct adaptive control strategy. Finally, a simulation study in Sec. VI demonstrates the performance of the adaptive control system compared with a nonadaptive controller in the presence of parametric uncertainties and modeling errors.

II. Dynamic Modeling

This Section first reviews the main equations of motion of rigid-joint robots and presents the linear joint stiffness equations of motion for a two-link flexible-joint manipulator. Then, the details of the derivation of the proposed nonlinear joint dynamics formulation are provided. In this paper, the linear joint model will be used for the design and preliminary validation of the adaptive controller performance, while the nonlinear joint model will be used to assess the robustness of the proposed adaptive control strategy to modeling errors.

As with previous studies on the control of flexible space manipulators [1–7], an inertially-stabilized platform (fixed base) assumption is adopted in this work.

A. Rigid Dynamics

A typical closed form of the nonlinear dynamics of a multilink robot with rigid joints is derived in terms of kinetic and potential energies stored in the system by the Euler–Lagrange formulation [36]. Given an independent set of generalized coordinates, where n is the number of DOF of the system, the total kinetic and potential energies stored in the rigid n-DOF system, T_r and U_r, respectively, are defined by the Lagrangian:

$$L(q_i, \dot{q}_i) = T_r - U_r, \qquad i = 1, \ldots, n \tag{1}$$

where the gravitational potential energy is omitted for space robot applications. For a robot subjected to a generalized force τ_i acting on the generalized coordinates q_i, the nonlinear dynamics equations of motion are given by

$$\tau_i = \frac{\mathrm{d}}{\mathrm{d}t}\left(\frac{\partial L}{\partial \dot{q}_i}\right) - \frac{\partial L}{\partial q_i}, \qquad i = 1, \ldots, n \tag{2}$$

The kinetic energy is calculated by the following quadratic form:

$$T_r = \frac{1}{2}\sum_{i=1}^{n}\sum_{j=1}^{n} M_{ij}\dot{q}_i\dot{q}_j = \frac{1}{2}\dot{\mathbf{q}}^T\mathbf{M}(\mathbf{q})\dot{\mathbf{q}} \tag{3}$$

where M_{ij} represents the components of the $n \times n$ symmetric positive-definite link inertia matrix $\mathbf{M}(\mathbf{q})$, and $\mathbf{q}$ is the link angle vector. Hence, the Euler–Lagrange rigid-dynamics equations of a n-DOF rigid-joint manipulator is

$$\mathbf{M}(\mathbf{q})\ddot{\mathbf{q}} + \mathbf{C}(\mathbf{q}, \dot{\mathbf{q}})\dot{\mathbf{q}} = \boldsymbol{\tau} \tag{4}$$

where $\mathbf{C}(\mathbf{q}, \dot{\mathbf{q}})$ represents the centrifugal-Coriolis matrix, and $\boldsymbol{\tau}$ represents the control torque vector. For the two-link robot shown in Fig. 1, $\mathbf{M}(\mathbf{q})$ and $\mathbf{C}(\mathbf{q}, \dot{\mathbf{q}})$ are given by [36]

$$\mathbf{M}(\mathbf{q}) = \begin{bmatrix} m_1 l_{c1}^2 + m_2(l_1^2 + l_{c2}^2 + 2l_1 l_{c2}\cos q_2) + I_1 + I_2 & m_2(l_{c2}^2 + l_1 l_{c2}\cos q_2) + I_2 \\ m_2(l_{c2}^2 + l_1 l_{c2}\cos q_2) + I_2 & m_2 l_{c2}^2 + I_2 \end{bmatrix} \tag{5}$$

$$\mathbf{C}(\mathbf{q}, \dot{\mathbf{q}}) = -m_2 l_1 l_{c2}\sin q_2 \begin{bmatrix} \dot{q}_2 & \dot{q}_1 + \dot{q}_2 \\ -\dot{q}_1 & 0 \end{bmatrix} \tag{6}$$

where, for $i = 1, 2$, l_i denotes the length of link i, l_{ci} denotes the distance from the previous joint to the center of gravity of link i, and m_i denotes the mass of link i. The moment of inertia of link i about an axis perpendicular to the xy plane passing through the center of gravity of link i, I_i, is given by

$$I_i = \frac{m_i l_i^2}{12} \tag{7}$$

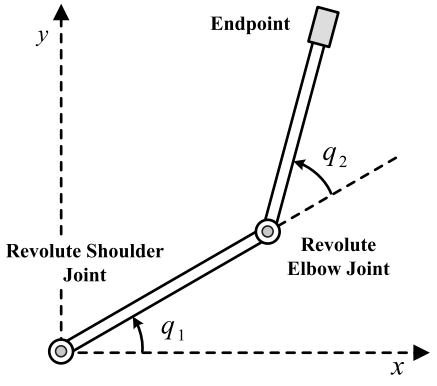

Fig. 1 Schematic of the two-link manipulator.

B. Linear Joint Stiffness Dynamics

Similar to the rigid-joint model, the well-known dynamics equations proposed by Spong [29] for robots with links elastically coupled to the link actuators (i.e., the rotors of dc motors) are derived in terms of kinetic and potential energies stored in the system by the Euler–Lagrange formulation. In this model, each joint is modeled as a linear torsional spring of constant stiffness, and the resulting dynamics of flexible-joint manipulators consist of two second-order differential equations. Because of the introduction of the elastic coupling between the motor shafts and the links, the dynamics model has n-DOF link dynamics and n-DOF motor dynamics. The ith flexible joint, in which the rotor is directly coupled to its link, is shown schematically in Fig. 2. Referring to this figure, let $\mathbf{q}_m$ be the vector denoting the angular displacements of the motor shaft angles, where the elastic joint vibration vector is defined as $\mathbf{q} - \mathbf{q}_m$. The joint flexibility effect is taken into account by augmenting the kinetic energy of the rigid-joint robot with the kinetic energy of each rotor, which is assumed to be due to their own rotation only, and by considering the elastic potential energy of the flexible joints. The kinetic energy of the rotors, T_e, and the elastic potential energy, U_e, are given, respectively, by

$$T_e = \frac{1}{2}\sum_{i=1}^{n}\sum_{j=1}^{n} J_{mij}\dot{q}_{mi}\dot{q}_{mj} = \frac{1}{2}\dot{\mathbf{q}}_m^T \mathbf{J}_m \dot{\mathbf{q}}_m \tag{8}$$

$$U_e = \frac{1}{2}\sum_{i=1}^{n}\sum_{j=1}^{n} k_{ij}(q_i - q_{mi})(q_j - q_{mj}) = \frac{1}{2}(\mathbf{q} - \mathbf{q}_m)^T \mathbf{k}(\mathbf{q} - \mathbf{q}_m) \tag{9}$$

where $\mathbf{J}_m$ denotes the positive-definite motor inertia matrix and where the stiffness of the flexible joints is modeled by $\mathbf{k}$, the diagonal positive-definite stiffness matrix of the joints. Combining elastic terms with rigid-dynamics equations, the following dynamics equations of a flexible-joint robot with revolute joints and actuated directly by dc motors are obtained:

$$\mathbf{M}(\mathbf{q})\ddot{\mathbf{q}} + \mathbf{C}(\mathbf{q}, \dot{\mathbf{q}})\dot{\mathbf{q}} - \mathbf{k}(\mathbf{q}_m - \mathbf{q}) = \mathbf{0} \tag{10}$$

$$\mathbf{J}_m\ddot{\mathbf{q}}_m + \mathbf{k}(\mathbf{q}_m - \mathbf{q}) = \boldsymbol{\tau} \tag{11}$$

In such a dynamics model, the link dynamics (10) and the actuator dynamics (11) are only coupled by the elastic torque term $\mathbf{k}(\mathbf{q}_m - \mathbf{q})$.

C. Nonlinear Joint Stiffness Dynamics

Since the development of the linear joint stiffness model, several experiments have been conducted to increase understanding of flexible effects in the joints of robotic manipulators, as their accurate modeling is key to the successful design of advanced flexible-joint control laws. The most relevant nonlinear effects are related to nonlinear joint stiffness. To replicate experimental joint stiffness curves, most researchers [31,32] recommend approximating the stiffness torque using a nonlinear cubic function, while others suggest a simple piecewise linear stiffness curve approximation [33].

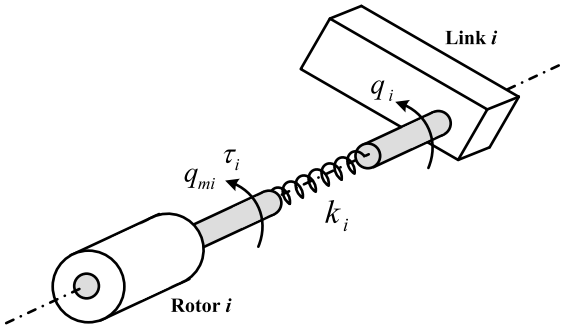

Fig. 2 Flexible-joint modeling.

An experiment confirmed that the nonlinear cubic model better represents nonlinear stiffness effects [34]. Therefore, in Eq. (10) the term $\mathbf{k}(\mathbf{q}_m - \mathbf{q})$ is replaced by a nonlinear cubic function [34]:

$$\mathbf{k}(\mathbf{q}, \mathbf{q}_m)(\mathbf{q}_m - \mathbf{q}) = \mathbf{a}_1 \begin{bmatrix} (q_{m1} - q_1)^3 \\ (q_{m2} - q_2)^3 \end{bmatrix} + \mathbf{a}_2(\mathbf{q}_m - \mathbf{q}) \tag{12}$$

Another important characteristic related to nonlinear joint stiffness was demonstrated in experiments by Kircanski and Goldenberg [30]. The authors observed that the torque-torsion characteristic is deformed toward the torque axis in the region from 0 to 1 N · m. In this region, the stiffness is lower due to the soft-windup effect, which can be mathematically modeled as a saddle-shaped function, as follows [30]:

$$\mathbf{K}_{\mathrm{sw}}(\mathbf{q}, \mathbf{q}_m) = -\mathbf{k}_{\mathrm{sw}} \begin{bmatrix} e^{-a_{\mathrm{sw}}(q_{m1} - q_1)^2} & 0 \\ 0 & e^{-a_{\mathrm{sw}}(q_{m2} - q_2)^2} \end{bmatrix} \tag{13}$$

where $\mathbf{k}_{\mathrm{sw}}$ and a_{sw}, respectively, are the diagonal positive-definite matrix and the parameter defining the soft-windup function.

In addition to nonlinear stiffness effects, it was determined that friction could not be neglected and must be modeled appropriately [37]. In the literature, several models of friction in flexible-joint mechanisms are available, most of them developed to reproduce friction curves observed in previous experiments. In this paper, the continuous and symmetric friction model proposed by Makkar et al. [38] was selected. The friction model is given by [38]

$$\boldsymbol{f}(\dot{\mathbf{q}}) = \gamma_1[\tanh(\gamma_2\dot{\mathbf{q}}) - \tanh(\gamma_3\dot{\mathbf{q}})] + \gamma_4 \tanh(\gamma_5\dot{\mathbf{q}}) + \gamma_6\dot{\mathbf{q}} \tag{14}$$

where, for $i = 1, \ldots, 6$, γ_i denotes positive parameters defining the different friction components. Compared with other experimental-based friction models, this specific formulation offers two advantages. First, it efficiently captures major nonlinear friction effects observed in experiments (static, kinetic, viscous, and Stribeck friction) without involving discontinuous or piecewise continuous functions. Indeed, most friction models are either discontinuous or only piecewise continuous, which can be problematic in the development of real-time estimation and control systems. Second, this symmetric continuous experimental-based friction model was successfully validated in actual flexible-joint manipulator experiments that required accurate estimation and control (see [39,40]), thus indicating that friction effects in flexible-joint mechanisms can be efficiently described by the continuous and symmetric model given by Eq. (14). Other experimental evidences that symmetric friction models are appropriate for flexible-joint manipulator applications include [41].

Another extension to the linear joint stiffness model can be made by removing the simplifying assumption of Spong's model regarding the kinetic energy of the rotors. In reality, the kinetic energy of the second rotor is also influenced by the rotation of the first link $\dot{q}_1$, that is,

$$T_{e2} = \frac{1}{2}J_{m2}(\dot{q}_1^2 + \dot{q}_{m2}^2) \tag{15}$$

In view of the above discussion, the following nonlinear dynamic model for flexible-joint manipulator systems, which overcomes the limitations of the model Eq. (10) and (11) by using prior experimental knowledge, is obtained herein as follows:

$$\mathbf{M}(\mathbf{q})\ddot{\mathbf{q}} + \mathbf{S}\ddot{\mathbf{q}}_m + \mathbf{C}(\mathbf{q}, \dot{\mathbf{q}})\dot{\mathbf{q}} + \boldsymbol{f}(\dot{\mathbf{q}}) - \mathbf{k}(\mathbf{q}, \mathbf{q}_m)(\mathbf{q}_m - \mathbf{q}) = \mathbf{0} \tag{16}$$

$$\mathbf{S}^T\ddot{\mathbf{q}} + \mathbf{J}_m\ddot{\mathbf{q}}_m + \mathbf{k}(\mathbf{q}, \mathbf{q}_m)(\mathbf{q}_m - \mathbf{q}) = \boldsymbol{\tau} \tag{17}$$

where the strictly upper triangular matrix $\mathbf{S}$ represents inertial couplings between motor and link accelerations introduced by the dependency of the second rotor's kinetic energy on the first link's angular velocity. The last term on the left side of Eq. (17) can be rewritten as

$$\mathbf{k}(\mathbf{q},\mathbf{q}_m)(\mathbf{q}_m-\mathbf{q})=\mathbf{a}_1\begin{bmatrix}(q_{m1}-q_1)^3\\(q_{m2}-q_2)^3\end{bmatrix}+\mathbf{a}_2(\mathbf{q}_m-\mathbf{q})-\mathbf{k}_{\mathrm{sw}}\begin{bmatrix}e^{-a_{\mathrm{sw}}(q_{m1}-q_1)^2}&0\\0&e^{-a_{\mathrm{sw}}(q_{m2}-q_2)^2}\end{bmatrix}(\mathbf{q}_m-\mathbf{q}) \tag{18}$$

Unlike Spong's model [29], the resulting nonlinear joint dynamics representation given by Eqs. (14–18) efficiently captures the nonlinear joint stiffness, soft-windup effect, friction torques, and inertial coupling previously observed in experiments and is therefore more suitable for the numerical validation of control systems. In the literature, similar comprehensive dynamics models have been used twice for the validation of flexible-joint control systems: first by Moghaddam and Goldenberg [42] to validate an H_∞ controller and then by ElMaraghy et al. [41] to assess the performance of a linear robust controller designed with linear-quadratic-Gaussian/loop-transfer-recovery techniques. However, the first neglects the inertial coupling and assumes only static and viscous friction terms, and the second neglects the soft-windup effect and uses a simplified friction model, which is linear in its parameters.

III. Background

For completeness, this section presents a summary of the simple adaptive control (SAC) and modified simple adaptive control (MSAC) theories. For a more detailed derivation of the SAC theory, refer to the work of Kaufman et al. [28] and Barkana [43]. More details about the MSAC approach can be found in Ulrich and de Lafontaine [27].

A. Simple Adaptive Control

The problem of self-adjusting the gains of a controller using an adaptation law in order to obtain the desired closed-loop characteristics, as defined by a reference model, is the idea behind direct model reference adaptive control (MRAC). Most standard MRAC adaptation laws assume prior knowledge of the unknown controlled plant order and require the use of models of the same order as the plant. Since this assumption may not always be valid in actual systems, a less complex MRAC adaptation law, known as simple adaptive control (SAC), was developed by Sobel et al. [44], Barkana et al. [45], and Barkana and Kaufman [46,47]. This direct adaptive method requires the plant, which could be of very large dimension, to track an ideal model, without requiring the model to be of the same order as the plant. In fact, the model is a representation of the plant only as far as its outputs represents the desired output behavior of the plant. This ideal model can be a first-order low-pass filter or a linear system large enough to generate the desired command. Thus, the ideal model is a command generator, and SAC is closely related to the command generator tracker approach. In the last few decades, the SAC methodology has been used in many successful applications, such as autopilots [43], reconfigurable flight control systems [48], and reentry vehicles [49]. Advantages of the SAC methodology, as compared with other MRAC adaptation laws, include that it is applicable to nonminimum phase systems, it is an output feedback method that requires neither full state feedback nor observers, and it does not require a mathematical model of the system to be controlled.

Let the nonlinear plant of order n_p be described by the following state-space representation:

$$\dot{\mathbf{x}}_p=\mathbf{A}_p\mathbf{x}_p+\mathbf{B}_p\mathbf{u}_p \tag{19}$$

$$\mathbf{y}_p=\mathbf{C}_p\mathbf{x}_p \tag{20}$$

The plant is required to track the output of the following model:

$$\dot{\mathbf{x}}_m=\mathbf{A}_m\mathbf{x}_m+\mathbf{B}_m\mathbf{u}_m \tag{21}$$

$$\mathbf{y}_m=\mathbf{C}_m\mathbf{x}_m \tag{22}$$

This model is allowed to be of any order n_m, just sufficiently large to create the desired response to the plant.

The input $\mathbf{u}_m$ is the signal that excites the ideal model such that its output $\mathbf{y}_m$ is the desired response. When full knowledge of the plant parameters cannot be assumed or when it is suspected that variable gains might be required in a particular environment, the SAC algorithm can be used to vary the control gains. In the SAC methodology, the control input $\mathbf{u}_p$ is given by

$$\mathbf{u}_p=\mathbf{K}_e(t)[\mathbf{y}_m-\mathbf{y}_p]+\mathbf{K}_x(t)\mathbf{x}_m+\mathbf{K}_u(t)\mathbf{u}_m \tag{23}$$

where $\mathbf{K}_e(t)$ is a stabilizing gain, and $\mathbf{K}_x(t)$ and $\mathbf{K}_u(t)$ are feedforward gains. These gains are varied in real time by an algorithm that must maintain stability of the controlled system and bring the tracking error to zero. The plant tracks the model perfectly when it moves along the ideal trajectory $\mathbf{x}_p^*$; otherwise, there is a state error $\mathbf{e}_x$ between the ideal trajectory and the actual trajectory:

$$\mathbf{e}_x=\mathbf{x}_p^*-\mathbf{x}_p \tag{24}$$

The output tracking error is defined as

$$\mathbf{e}_y=\mathbf{y}_m-\mathbf{y}_p=\mathbf{C}_p\mathbf{x}_p^*-\mathbf{C}_p\mathbf{x}_p=\mathbf{C}_p\mathbf{e}_x \tag{25}$$

This output tracking error is used to generate integral adaptive control gains, as follows:

$$\dot{\mathbf{K}}_{Ix}(t)=\mathbf{e}_y\mathbf{x}_m^T\Gamma_{Ix} \tag{26}$$

$$\dot{\mathbf{K}}_{Iu}(t)=\mathbf{e}_y\mathbf{u}_m^T\Gamma_{Iu} \tag{27}$$

$$\dot{\mathbf{K}}_{Ie}(t)=\mathbf{e}_y\mathbf{e}_y^T\Gamma_{Ie} \tag{28}$$

where Γ_{Ix}, Γ_{Iu}, and Γ_{Ie} are constant coefficient matrices that control the rate of adaptation. Equations (26–28) can be written concisely by defining

$$\mathbf{K}_I(t)=[\,\mathbf{K}_{Ie}(t)\quad\mathbf{K}_{Ix}(t)\quad\mathbf{K}_{Iu}(t)\,] \tag{29}$$

$$\mathbf{r}=[\,\mathbf{e}_y\quad\mathbf{x}_m\quad\mathbf{u}_m\,]^T \tag{30}$$

With this notation, $\dot{\mathbf{K}}_I(t)$ is given by

$$\dot{\mathbf{K}}_I(t)=\mathbf{e}_y\mathbf{r}^T\Gamma_I \tag{31}$$

where Γ_I is the resulting adaptation coefficients for the combined integral gain $\mathbf{K}_I(t)$. It should be noted that although only the integral adaptive gain $\mathbf{K}_I(t)$ is absolutely necessary to guarantee the convergence of the adaptive control system, it is preferable to use the proportional adaptive gain $\mathbf{K}_p(t)$ as well, in order to increase the rate of convergence of the adaptive system toward perfect tracking. For this reason, it is common practice to include $\mathbf{K}_p(t)$, which is defined as

$$\mathbf{K}_p(t)=[\,\mathbf{K}_{pe}(t)\quad\mathbf{K}_{px}(t)\quad\mathbf{K}_{pu}(t)\,]=\mathbf{e}_y\mathbf{r}^T\Gamma_p \tag{32}$$

Hence, the total adaptive gain is

$$\mathbf{K}(t)=[\,\mathbf{K}_e(t)\quad\mathbf{K}_x(t)\quad\mathbf{K}_u(t)\,]=\mathbf{K}_I(t)+\mathbf{K}_p(t)$$

Finally, the SAC control law can be rewritten as

$$\mathbf{u}_p=\mathbf{K}(t)\mathbf{r} \tag{33}$$

B. Modified Simple Adaptive Control

The greatest difficulty in designing the SAC controller is determining the various weighting matrix coefficients. The SAC theory does not provide any means of efficiently selecting the several coefficients of the weighting matrices, although Kaufman et al. [28] do give some recommendations. To overcome this design complexity

and to further decrease the number of required operations needed to implement the SAC algorithm in real time, Ulrich and de Lafontaine [27] derived a modified version of the SAC algorithm, referred to as the modified simple adaptive control (MSAC) law. The MSAC algorithm is obtained by keeping only the error-related adaptive gains, $\mathbf{K}_{pe}(t)$ and $\mathbf{K}_{Ie}(t)$, in Eqs. (29) and (32). In fact, as explained by Barkana et al. [47], only $\mathbf{K}_e(t)$ is absolutely required for the stability of the adaptive system. The resulting MSAC adaptation law is given by

$$\mathbf{u}_p = \mathbf{K}_e(t)\mathbf{e}_y \tag{34}$$

with the proportional and integral components of $\mathbf{K}_e(t)$ defined as

$$\mathbf{K}_{pe}(t) = \mathbf{e}_y\mathbf{e}_y^T\Gamma_p \tag{35}$$

$$\dot{\mathbf{K}}_{Ie}(t) = \mathbf{e}_y\mathbf{e}_y^T\Gamma_I \tag{36}$$

Compared with SAC, the MSAC methodology has the advantage of requiring less computation power while providing similar tracking performance [50]. In this paper, in order to further decrease the number of computations associated with MSAC, a local decentralized control that keeps only the diagonal elements of $\mathbf{e}_y\mathbf{e}_y^T$ is considered.

IV. Direct Adaptive Controller Formulation

The proposed trajectory-tracking strategy uses the SPB theory, which transforms a dynamics model into a two-timescale model: specifically, the quasi-steady-state model and the boundary-layer model. Here, for brevity, only the final results of the approach are presented. A more comprehensive treatment of the SPB theory is given by Khalil [19] and a survey of its application to aerospace systems can be found in [51]. The robot quasi-steady-state model is

$$\mathbf{H}(\mathbf{q}_s)\ddot{\mathbf{q}}_s + \mathbf{C}(\mathbf{q}_s, \dot{\mathbf{q}}_s)\dot{\mathbf{q}}_s = \boldsymbol{\tau}_s \tag{37}$$

where $\mathbf{H}(\mathbf{q}_s) = \mathbf{M}(\mathbf{q}_s) + \mathbf{J}_m$ and the subscripts s stand for slow variables defined in the slow time scale t. When applied to flexible-joint robots, the SPB theory provides a framework to design adaptive composite controllers, in which the motor torque control input is given by $\boldsymbol{\tau} = \boldsymbol{\tau}_s + \boldsymbol{\tau}_f$, where the subscripts f stand for variables defined in the fast time scale $t' = t/\epsilon$, with ϵ being a small positive parameter. The slow control torque $\boldsymbol{\tau}_s$ is applied to the quasi-steady-state model, and the fast-control torque $\boldsymbol{\tau}_f$ is applied to the boundary-layer model to provide additional damping of the elastic vibrations at the joints. The fast-control torque chosen herein is a linear correction of the form

$$\boldsymbol{\tau}_f = \mathbf{K}_v(\dot{\mathbf{q}} - \dot{\mathbf{q}}_m) \tag{38}$$

where $\mathbf{K}_v$ is a control gain.

Note that the quasi-steady-state model given by Eq. (37) is equivalent to the rigid-joint dynamics shown in Eq. (4). In this paper, stabilization of the quasi-steady-state dynamics is achieved by applying a Cartesian-based control scheme. When the desired trajectory is specified in terms of end-effector Cartesian position and velocity, i.e., in the task space, and requires precise control of the end-effector motion, joint-space control schemes are usually not suitable. Joint-based control schemes refers to controllers in which the feedback is based on joint positions and velocities, such that the control error is defined in terms of $\mathbf{q}_d - \mathbf{q}$ and $\dot{\mathbf{q}}_d - \dot{\mathbf{q}}$. On the other hand, with Cartesian-based control schemes, the actual Cartesian description of the end effector, which may be directly measured or computed from joint positions and velocities by means of the direct kinematic equations, is compared with the desired Cartesian trajectory in order to form errors in the task space. Cartesian-based control schemes are then those driven by Cartesian position errors instead of joint position or velocity errors. The main practical advantage of Cartesian-based controllers is that the solution of the inverse kinematics and inverse Jacobian, required to transform the desired end-effector position and velocity into $\mathbf{q}_d$ and $\dot{\mathbf{q}}_d$, is removed. One of most popular Cartesian-based controllers is the transpose Jacobian control law, first developed by Craig [52]. However, the selection of the control gains is a problem with this rigid-joint control law. As a result, tuning is conducted by tedious trial and error procedure. It was also observed that, depending on the desired Cartesian trajectory, retuning of the gains is required, which is a severe drawback of this controller and unacceptable in practical applications. This motivates the development of an adaptive approach in which the control parameters are automatically adjusted in real time, according to the MSAC adaptation law, in order to minimize the differences between the ideal and actual plant outputs. This way, the tracking performance of the controller is less sensitive to uncertainties in the actual system. The adaptive control law proposed to stabilize the quasi-steady-state model is given by

$$\boldsymbol{\tau}_s = \mathbf{J}(\mathbf{q})^T\left[\mathbf{K}_p(t)\begin{pmatrix} x_e \\ y_e \end{pmatrix} + \mathbf{K}_d(t)\begin{pmatrix} \dot{x}_e \\ \dot{y}_e \end{pmatrix}\right] \tag{39}$$

where $\mathbf{K}_p(t)$ and $\mathbf{K}_d(t)$ are the proportional and derivative adaptive control gain matrices, respectively. Alternatively, the adaptive control law can be rewritten in standard MSAC form, as follows:

$$\boldsymbol{\tau}_s = \mathbf{J}(\mathbf{q})^T\mathbf{K}_e(t)\mathbf{e}_y \tag{40}$$

with

$$\mathbf{K}_e(t) = [\,\mathbf{K}_p(t) \quad \mathbf{K}_d(t)\,] = \mathbf{K}_{pe}(t) + \mathbf{K}_{Ie}(t) \tag{41}$$

The proportional and integral components of the adaptive control gain, $\mathbf{K}_{pe}(t)$ and $\mathbf{K}_{Ie}(t)$, respectively, are defined accordingly to the MSAC methodology. Adopting a local decentralized control approach, these adaptive gains are given by

$$\mathbf{K}_{pe}(t) = \begin{bmatrix} x_e^2\Gamma_{pp} & 0 & \dot{x}_e^2\Gamma_{dp} & 0 \\ 0 & y_e^2\Gamma_{pp} & 0 & \dot{y}_e^2\Gamma_{dp} \end{bmatrix} \tag{42}$$

$$\dot{\mathbf{K}}_{Ie}(t) = \begin{bmatrix} x_e^2\Gamma_{pi} - \sigma_p K_{Ie_{11}}(t) & 0 & \dot{x}_e^2\Gamma_{di} - \sigma_d K_{Ie_{13}}(t) & 0 \\ 0 & y_e^2\Gamma_{pi} - \sigma_p K_{Ie_{22}}(t) & 0 & \dot{y}_e^2\Gamma_{di} - \sigma_d K_{Ie_{24}}(t) \end{bmatrix} \tag{43}$$

In Eqs. (42) and (43), Γ_{pp}, Γ_{pi}, Γ_{dp}, and Γ_{di} are parameters that control the adaptation rate of the controller. By adopting Ioannou and Kokotovik's [53] idea, the coefficients σ_p and σ_d are introduced. With this adjustment, the integral gains increase as required (due to large tracking errors, for example) and decrease when large gains are no longer necessary. These coefficients must be set between 0 and 1 to avoid divergence of the integral control gains. Indeed, if these coefficients are set to zero, the integral adaptive gains would increase for as long as there is a tracking error. When the integral gains reach some values, they have a stabilizing effect on the system and the tracking error starts decreasing. However, if, for some reasons, the tracking error does not reach zero, the integral gains would continue to increase. Furthermore, every sudden change in the commanded trajectory would generate greater values of these adaptive gains and

could lead to instability. On the other hand, if both coefficients are set between 0 and 1, the integral adaptive gains are obtained from a first-order filtering of the tracking error and cannot diverge unless the error diverges.

By combining the slow and the fast-control term defined previously, the controller that actuates each joint is obtained as follows:

$$\boldsymbol{\tau} = \mathbf{J}(\mathbf{q})^T \mathbf{K}_e(t)\mathbf{e}_y + \mathbf{K}_v(\dot{\mathbf{q}} - \dot{\mathbf{q}}_m) \tag{44}$$

This control torque feeds into the inverse flexible-joint dynamics equations, resulting in a link and motor angular acceleration vectors $\ddot{\mathbf{q}}$ and $\ddot{\mathbf{q}}_m$, which are double-integrated to obtain link and motor velocities $\dot{\mathbf{q}}$ and $\dot{\mathbf{q}}_m$ and link and motor positions $\mathbf{q}$ and $\mathbf{q}_m$. The error between link and motor velocities is used in the fast-control term to add additional damping of the elastic vibrations at the joints. The position of the flexible robot end effector with respect to the robot reference frame is denoted by

$$\begin{bmatrix} x_p \\ y_p \end{bmatrix} = \Omega(\mathbf{q}) \tag{45}$$

where $\Omega(\mathbf{q})$ is the forward kinematic transformation taking joint angular positions into Cartesian position. The differential kinematics is obtained as the time derivative of the forward kinematics (45) as follows:

$$\begin{bmatrix} \dot{x}_p \\ \dot{y}_p \end{bmatrix} = \mathbf{J}(\mathbf{q})\dot{\mathbf{q}} \tag{46}$$

where the analytical Jacobian matrix $\mathbf{J}(\mathbf{q})$ is defined by

$$\mathbf{J}(\mathbf{q}) = \frac{\partial \Omega(\mathbf{q})}{\partial \mathbf{q}} \tag{47}$$

Combining Eqs. (45) and (46), the joint-space dynamics are then transformed into the task-space dynamics through the transformation [36]

$$\mathbf{y}_p = \begin{bmatrix} x_p \\ y_p \\ \dot{x}_p \\ \dot{y}_p \end{bmatrix} = \begin{bmatrix} l_1\cos(q_1) + l_2\cos(q_1+q_2) \\ l_1\sin(q_1) + l_2\sin(q_1+q_2) \\ -l_1\sin(q_1)\dot{q}_1 - l_2\sin(q_1+q_2)(\dot{q}_1+\dot{q}_2) \\ l_1\cos(q_1)\dot{q}_1 + l_2\cos(q_1+q_2)(\dot{q}_1+\dot{q}_2) \end{bmatrix} \tag{48}$$

Following common practices, the desired time-varying trajectory for the robot end-effector position and velocity is specified in the task space, i.e., $\mathbf{u}_m = [\,x_d \quad y_d \quad \dot{x}_d \quad \dot{y}_d\,]^T$. Thus, this desired trajectory is used as the input of the ideal model described as

$$\dot{\mathbf{x}}_m = \begin{bmatrix} \dot{x}_m \\ \dot{y}_m \\ \ddot{x}_m \\ \ddot{y}_m \end{bmatrix} = \begin{bmatrix} 0 & 0 & 0 & 0 \\ 0 & 0 & 0 & 0 \\ -\omega_n^2 & 0 & -2\xi\omega_n & 0 \\ 0 & -\omega_n^2 & 0 & -2\xi\omega_n \end{bmatrix} \begin{bmatrix} x_m \\ y_m \\ \dot{x}_m \\ \dot{y}_m \end{bmatrix} + \begin{bmatrix} 0 & 0 & 1 & 0 \\ 0 & 0 & 0 & 1 \\ \omega_n^2 & 0 & 0 & 0 \\ 0 & \omega_n^2 & 0 & 0 \end{bmatrix} \mathbf{u}_m \tag{49}$$

The output vector of this ideal model, $\mathbf{y}_m = [\,x_m \quad y_m \quad \dot{x}_m \quad \dot{y}_m\,]^T$, is compared with the flexible-joint robot end-effector position and velocity vectors described in the task-space coordinates, $\mathbf{y}_p = [\,x_p \quad y_p \quad \dot{x}_p \quad \dot{y}_p\,]^T$, to establish the tracking errors between them, $\mathbf{e}_y = [\,x_e \quad y_e \quad \dot{x}_e \quad \dot{y}_e\,]^T$, that is,

$$\mathbf{e}_y = \mathbf{y}_m - \mathbf{y}_p = \begin{bmatrix} x_m - x_p \\ y_m - y_p \\ \dot{x}_m - \dot{x}_p \\ \dot{y}_m - \dot{y}_p \end{bmatrix} = \begin{bmatrix} x_e \\ y_e \\ \dot{x}_e \\ \dot{y}_e \end{bmatrix} \tag{50}$$

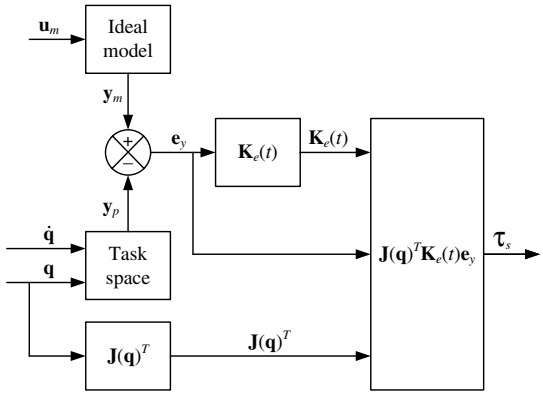

Fig. 3 Block scheme of the slow adaptive controller implementation.

This output tracking error vector is used in the adaptive controller to update the control gains according to the MSAC law. A block-scheme representation of the implementation of the slow adaptive control torque is given in Fig. 3.

V. Stability Analysis

It is known [19] that the stability of both the quasi-steady-state and boundary-layer subsystem can be analyzed separately, i.e., by applying $\boldsymbol{\tau}_f$ to the boundary-layer model and by applying $\boldsymbol{\tau}_s$ to the quasi-steady-state model. As far as the stability of the boundary-layer model is concerned, it was previously demonstrated, by invoking LaSalle's theorem, that a linear correction term of the form $\boldsymbol{\tau}_f = \mathbf{K}_v(\dot{\mathbf{q}} - \dot{\mathbf{q}}_m)$ is sufficient to ensure global asymptotic stability of the closed-loop boundary-layer subsystem [21].

The stability of the quasi-steady-state model under the rigid-based MSAC control law $\boldsymbol{\tau}_s$ presented herein follows closely the development presented in [28,47], which demonstrates the stability of the original SAC control law. For such adaptive control laws, it must first be shown that the system is almost strictly passive (ASP). An ASP system is defined as a system that can be stabilized through some constant output feedback $\tilde{\mathbf{K}}$ that is unknown and not required for implementation. As a result, a fictitious closed-loop ASP system with the system matrix

$$\mathbf{A}_{\mathrm{CL}} = \mathbf{A} - \mathbf{B}\tilde{\mathbf{K}}\mathbf{C} \tag{51}$$

satisfies the following passivity conditions for nonstationary and nonlinear systems [54]:

$$\dot{\mathbf{P}} + \mathbf{P}\mathbf{A}_{\mathrm{CL}} + \mathbf{A}_{\mathrm{CL}}^T\mathbf{P} = -\mathbf{Q} \tag{52}$$

$$\mathbf{P}\mathbf{B} = \mathbf{C}^T \tag{53}$$

Here, $\mathbf{P}$ and $\mathbf{Q}$ are positive-definite matrices. Since the fictitious closed-loop system satisfies the strict passivity (SP) conditions (52) and (53), the original system is called almost strictly passive (ASP), because only a constant output feedback gain separates it from strict passivity. As it will be shown in this section, the ASP conditions of the system to be controlled facilitate the derivation of its Lyapunov proof of stability. This section first demonstrates that the quasi-steady-state model is ASP, followed by a discussion of the stability of the adaptive system.

A. Almost Strictly Passive Property

The ASP property implies that the plant is minimum-phase (stable zero dynamics) and the product $\mathbf{C}_s\mathbf{B}_s$ is positive-definite. For convenience, the quasi-steady-state model of the robot is rewritten into the task-space dynamics, as follows [55]:

$$\boldsymbol{\Lambda}(\mathbf{q}_s)\ddot{\mathbf{x}}_s + \boldsymbol{\Pi}(\mathbf{q}_s, \dot{\mathbf{q}}_s)\dot{\mathbf{x}}_s = \mathbf{f}_s \tag{54}$$

where $\mathbf{f}_s$ denotes the command forces in the task space. The pseudoinertia matrix $\mathbf{\Lambda}(\mathbf{q}_s)$ is defined by

$$\mathbf{\Lambda}(\mathbf{q}_s) = \mathbf{J}^{-T}(\mathbf{q}_s)\mathbf{H}(\mathbf{q}_s)\mathbf{J}^{-1}(\mathbf{q}_s) \tag{55}$$

and $\mathbf{\Pi}(\mathbf{q}_s, \dot{\mathbf{q}}_s)$ is given by

$$\mathbf{\Pi}(\mathbf{q}_s, \dot{\mathbf{q}}_s) = \mathbf{J}^{-T}(\mathbf{q}_s)\mathbf{C}(\mathbf{q}_s, \dot{\mathbf{q}}_s)\mathbf{J}^{-1}(\mathbf{q}_s) - \mathbf{\Lambda}(\mathbf{q}_s)\mathbf{J}(\mathbf{q}_s)\mathbf{J}^{-1}(\mathbf{q}_s) \tag{56}$$

The quasi-steady-state model can then be expressed as a state-space representation:

$$\dot{\mathbf{x}}_s = \begin{bmatrix} \dot{x}_s \\ \dot{y}_s \\ \ddot{x}_s \\ \ddot{y}_s \end{bmatrix} = \begin{bmatrix} \mathbf{0} & \mathbf{I}_2 \\ \mathbf{0} & -\mathbf{\Lambda}(\mathbf{q}_s)^{-1}\mathbf{\Pi}(\mathbf{q}_s, \dot{\mathbf{q}}_s) \end{bmatrix}\mathbf{x}_s + \begin{bmatrix} \mathbf{0} \\ \mathbf{\Lambda}(\mathbf{q}_s)^{-1} \end{bmatrix}\mathbf{f}_s \tag{57}$$

$$\mathbf{C}_s = \mathbf{I}_4 \tag{58}$$

Since the ASP conditions have so far only been established for square systems, let the outputs of the quasi-steady-state model described above be a linear combination of the states, as follows:

$$\hat{\mathbf{C}}_s = [\,\mathbf{I}_2 \quad \mathbf{I}_2\,]\mathbf{C}_s \tag{59}$$

The nonstationary system defined by Eqs. (57) and (59) is defined as *uniformly strictly minimum-phase* or simply minimum-phase, if there are two matrices $\mathbf{M}$ and $\mathbf{N}$ satisfying [54]

$$\hat{\mathbf{C}}_s\mathbf{M} = \mathbf{0} \tag{60}$$

$$\mathbf{N}\,\mathbf{B}_s = \mathbf{0} \tag{61}$$

$$\mathbf{NM} = \mathbf{I}_2 \tag{62}$$

such that the zero dynamics given by

$$\dot{\mathbf{z}} = (\dot{\mathbf{N}} + \mathbf{NA}_s)\mathbf{Mz} \tag{63}$$

is uniformly asymptotically stable. A simple selection of matrices that satisfy Eqs. (60–62) is

$$\mathbf{M} = \begin{bmatrix} \mathbf{I}_2 \\ -\mathbf{I}_2 \end{bmatrix}, \qquad \mathbf{N} = [\,\mathbf{I}_2 \quad \mathbf{0}\,] \tag{64}$$

Computing

$$\mathbf{A}_z = \mathbf{NA}_s\mathbf{M} = -\mathbf{I}_2 \tag{65}$$

and thus

$$\dot{\mathbf{z}} = \mathbf{A}_z\mathbf{z} = -\mathbf{z} \tag{66}$$

which shows that the zero dynamics is stable and the quasi-steady-state model is minimum-phase. Moreover, it can easily be verified that the product $\hat{\mathbf{C}}_s\mathbf{B}_s$ is positive-definite by

$$\hat{\mathbf{C}}_s\mathbf{B}_s = [\,\mathbf{I}_2 \quad \mathbf{I}_2\,]\mathbf{C}_s\begin{bmatrix} \mathbf{0} \\ \mathbf{\Lambda}(\mathbf{q}_s)^{-1} \end{bmatrix} = \mathbf{\Lambda}(\mathbf{q}_s)^{-1} > \mathbf{0} \tag{67}$$

Therefore, the square quasi-steady-state model described by $\{\,\mathbf{A}_s \quad \mathbf{B}_s \quad \hat{\mathbf{C}}_s \quad \mathbf{0}\,\}$ is ASP, and the following conditions hold:

$$\dot{\mathbf{P}} + \mathbf{P}(\mathbf{A}_s - \mathbf{B}_s\tilde{\mathbf{K}}\hat{\mathbf{C}}_s) + (\mathbf{A}_s - \mathbf{B}_s\tilde{\mathbf{K}}\hat{\mathbf{C}}_s)^T\mathbf{P} = -\mathbf{Q} \tag{68}$$

$$\mathbf{P}\,\mathbf{B}_s = \hat{\mathbf{C}}_s^T \tag{69}$$

These two ASP conditions can also be rewritten in terms of the original nonsquare output matrix $\mathbf{C}_s$, as follows:

$$\dot{\mathbf{P}} + \mathbf{P}(\mathbf{A}_s - \mathbf{B}_s\tilde{\mathbf{K}}_e\mathbf{C}_s) + (\mathbf{A}_s - \mathbf{B}_s\tilde{\mathbf{K}}_e\mathbf{C}_s)^T\mathbf{P} = -\mathbf{Q} \tag{70}$$

$$\mathbf{P}\,\mathbf{B}_s = ([\,\mathbf{I}_2 \quad \mathbf{I}_2\,]\mathbf{C}_s)^T = \mathbf{C}_s^T\begin{bmatrix} \mathbf{I}_2 \\ \mathbf{I}_2 \end{bmatrix} \tag{71}$$

Hence, there is a constant output feedback $\tilde{\mathbf{K}}_e$ (e.g., $\tilde{\mathbf{K}}_e = \tilde{\mathbf{K}}[\,\mathbf{I}_2 \quad \mathbf{I}_2\,]$) that is unknown and not required for implementation that maintains the stability of the fictitious closed-loop system $\mathbf{A}_s - \mathbf{B}_s\tilde{\mathbf{K}}_e\mathbf{C}_s$ obtained from the original nonsquare $\{\,\mathbf{A}_s \quad \mathbf{B}_s \quad \mathbf{C}_s \quad \mathbf{0}\,\}$ system.

B. Model Following

The state error $\mathbf{e}_x$ between the ideal trajectory and the quasi-steady-state model trajectory is

$$\mathbf{e}_x = \mathbf{x}_s^* - \mathbf{x}_s = \begin{bmatrix} x_s^* \\ y_s^* \\ \dot{x}_s^* \\ \dot{y}_s^* \end{bmatrix} - \begin{bmatrix} x_s \\ y_s \\ \dot{x}_s \\ \dot{y}_s \end{bmatrix} \tag{72}$$

and the output tracking error is defined as

$$\mathbf{e}_y = \mathbf{y}_m - \mathbf{y}_s = \mathbf{C}_s\mathbf{x}_s^* - \mathbf{C}_s\mathbf{x}_s = \mathbf{C}_s\mathbf{e}_x \tag{73}$$

This tracking error is used directly in the adaptive controller given by

$$\boldsymbol{\tau}_s = \mathbf{J}(\mathbf{q}_s)^T\mathbf{K}_e(t)\mathbf{e}_y \tag{74}$$

which can be rewritten in terms of the control forces in the task space, $\mathbf{f}_s$, as follows:

$$\mathbf{f}_s = \mathbf{J}(\mathbf{q}_s)^{-T}\boldsymbol{\tau}_s = \mathbf{J}(\mathbf{q}_s)^{-T}[\mathbf{J}(\mathbf{q}_s)^T\mathbf{K}_e(t)\mathbf{e}_y] = \mathbf{K}_e(t)\mathbf{e}_y \tag{75}$$

Note that in the adaptive controller given by Eq. (74), the output tracking error $\mathbf{e}_y$ has been redefined in terms of the quasi-steady-state model outputs $\mathbf{y}_s$ instead of $\mathbf{y}_p$, and the variable $\mathbf{q}$ has been replaced by $\mathbf{q}_s$, since the stability of the slow subsystem is analyzed by applying $\boldsymbol{\tau}_s$ only to the quasi-steady-state model [19]. The gain $\mathbf{K}_e(t)$ is a combination of integral and proportional adaptive gains, as shown in Eq. (41). The resulting quasi-steady-state adaptive system is

$$\dot{\mathbf{x}}_s = \mathbf{A}_s\mathbf{x}_s + \mathbf{B}_s\mathbf{f}_s = \mathbf{A}_s\mathbf{x}_s + \mathbf{B}_s\mathbf{K}_e(t)\mathbf{e}_y \tag{76}$$

One can see that $\dot{\mathbf{K}}_{Ie}(t)$, given by Eq. (43), is equivalent to

$$\dot{\mathbf{K}}_{Ie}(t) = [\,\mathbf{I}_2 \quad \mathbf{I}_2\,]\mathrm{diag}(\mathbf{e}_y^2)\Gamma_I - \boldsymbol{\sigma}\mathrm{diag}[\mathbf{K}_{Ie}(t)] \tag{77}$$

with

$$\mathrm{diag}\,(\mathbf{e}_y^2) = \begin{bmatrix} x_e^2 & 0 & 0 & 0 \\ 0 & y_e^2 & 0 & 0 \\ 0 & 0 & \dot{x}_e^2 & 0 \\ 0 & 0 & 0 & \dot{y}_e^2 \end{bmatrix} \tag{78}$$

$$\mathrm{diag}\,[\mathbf{K}_{Ie}(t)] = \begin{bmatrix} K_{Ie_{11}}(t) & 0 & 0 & 0 \\ 0 & K_{Ie_{22}}(t) & 0 & 0 \\ 0 & 0 & K_{Ie_{13}}(t) & 0 \\ 0 & 0 & 0 & K_{Ie_{24}}(t) \end{bmatrix} \tag{79}$$

$$\Gamma_I = \begin{bmatrix} \Gamma_{pi} & 0 & 0 & 0 \\ 0 & \Gamma_{pi} & 0 & 0 \\ 0 & 0 & \Gamma_{di} & 0 \\ 0 & 0 & 0 & \Gamma_{di} \end{bmatrix} \tag{80}$$

$$\boldsymbol{\sigma} = \begin{bmatrix} \sigma_p & 0 & 0 & 0 \\ 0 & \sigma_p & 0 & 0 \\ 0 & 0 & \sigma_d & 0 \\ 0 & 0 & 0 & \sigma_d \end{bmatrix} \tag{81}$$

Similarly, Eq. (42) is equivalent to

$$\mathbf{K}_{pe}(t) = [\,\mathbf{I}_2 \quad \mathbf{I}_2\,]\mathrm{diag}(\mathbf{e}_y^2)\Gamma_p \tag{82}$$

Subtracting the plant equation from the ideal trajectory gives, after various algebraic manipulations, the following state error dynamics (see Appendix A for details):

$$\dot{\mathbf{e}}_x = (\mathbf{A}_s - \mathbf{B}_s\tilde{\mathbf{K}}_e\mathbf{C}_s)\mathbf{e}_x - \mathbf{B}_s\mathbf{K}_{pe}(t)\mathbf{e}_y - \mathbf{B}_s(\mathbf{K}_{Ie}(t) - \tilde{\mathbf{K}}_e)\mathbf{e}_y + (\mathbf{A}_s^* - \mathbf{A}_s)\mathbf{x}_s^* \tag{83}$$

The proof of stability must consider Eqs. (77) and (83), since, as shown by Kaufman et al. [28], only the integral adaptive gain is needed for stability of the adaptive system, yet the proportional gain has the effect of increasing the tracking performance, as demonstrated below.

The following positive-definite symmetric Lyapunov function will be used for the proof of stability:

$$V(\mathbf{e}_x, \mathbf{K}_{Ie}, t) = \mathbf{e}_x^T\mathbf{P}\mathbf{e}_x + \mathrm{tr}[(\mathbf{K}_{Ie}(t) - \tilde{\mathbf{K}}_e)\Gamma_I^{-1}(\mathbf{K}_{Ie}(t) - \tilde{\mathbf{K}}_e)^T] \tag{84}$$

Using ASP conditions (70) and (71), the derivative of the Lyapunov function is (see Appendix B for complete derivation)

$$\dot{V}(\mathbf{e}_x, \mathbf{K}_{Ie}, t) = -\mathbf{e}_x^T\mathbf{Q}\mathbf{e}_x - 2\sigma\,\mathrm{tr}[(\mathbf{K}_{Ie}(t) - \tilde{\mathbf{K}}_e)(\mathbf{K}_{Ie}(t) - \tilde{\mathbf{K}}_e)^T] - \mathbf{e}_y^T\left(\mathbf{K}_{pe}(t)[\,\mathbf{I}_2 \quad \mathbf{I}_2\,] + \begin{bmatrix}\mathbf{I}_2\\ \mathbf{I}_2\end{bmatrix}\mathbf{K}_{pe}(t)\right)\mathbf{e}_y + 2\mathbf{e}_x^T\mathbf{P}(\mathbf{A}_s^* - \mathbf{A}_s)\mathbf{x}_s^* - 2\sigma\,\mathrm{tr}[\tilde{\mathbf{K}}_e(\mathbf{K}_{Ie}(t) - \tilde{\mathbf{K}}_e)^T] \tag{85}$$

The first two terms are negative definite in terms of $\mathbf{e}_x$ and $\mathbf{K}_{Ie}(t)$, respectively, whereas the last two terms are not definite; one of these being due to the introduction of the σ term to guarantee robustness of the adaptive algorithm. Hence, one can only claim bounded error tracking instead of asymptotic tracking although, as the application in the next section shows, the tracking errors ultimately converge. Also, though the integral adaptive gain is sufficient for the stability of the adaptive system, the negative definite term in $\mathbf{e}_y$ introduced by including the proportional adaptive gain $\mathbf{K}_{pe}(t)$ in the controller adds to the negativity of the Lyapunov derivative and thus to the rate of convergence of the error.

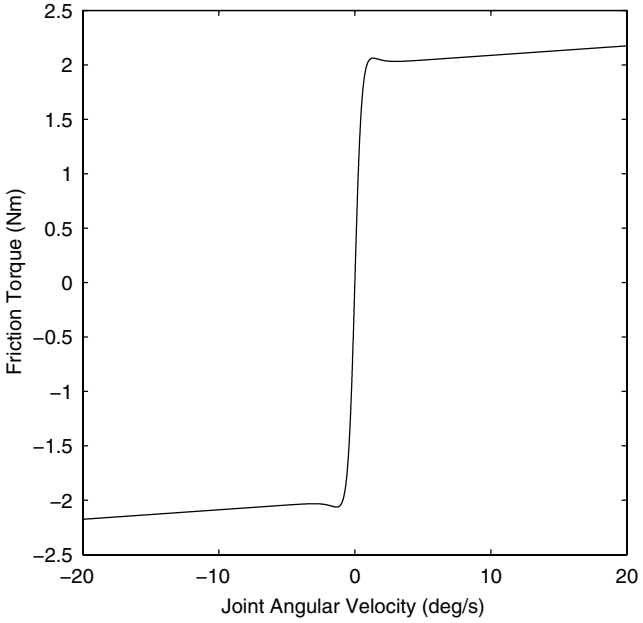

Fig. 5 Friction curve.

VI. Numerical Simulations

This section presents the numerical simulation results obtained by implementing the adaptive composite controller developed in this paper. The physical properties of the robot (the length and the mass of the links) are adopted from previous studies on intelligent control of space robots [2,3], and the flexible parameters are based on [26], which are representative of manipulators with obvious flexible-joint effects. The parameters of the two-link flexible-joint robot are summarized as follows: $l_1 = l_2 = 4.5$ m, $m_1 = m_2 = 1.5075$ kg, $\mathbf{J}_m = \mathrm{diag}[1]\ \mathrm{kg}\cdot\mathrm{m}^2$ and $\mathbf{k} = \mathrm{diag}[500]\mathrm{N}\cdot\mathrm{m/rad}$. The parameters for the nonlinear joint dynamics model are selected as $\mathbf{a}_1 = \mathbf{a}_2 = \mathrm{diag}[500]\mathrm{N}\cdot\mathrm{m/rad}$, $\mathbf{k}_{\mathrm{sw}} = \mathrm{diag}[10]$, $a_{\mathrm{sw}} = 3000$, $\gamma_1 = 0.5$, $\gamma_2 = 150$, $\gamma_3 = 50$, $\gamma_4 = 2$, $\gamma_5 = 100$, and $\gamma_6 = 0.5$. The inertial coupling matrix is $\mathbf{S} = \begin{bmatrix}0 & J_{m2}\\ 0 & 0\end{bmatrix}$. With these parameters, the nonlinear joint stiffness and friction curves are given in Figs. 4 and 5, respectively, where the joint torsion is defined as $\mathbf{q}_m - \mathbf{q}$.

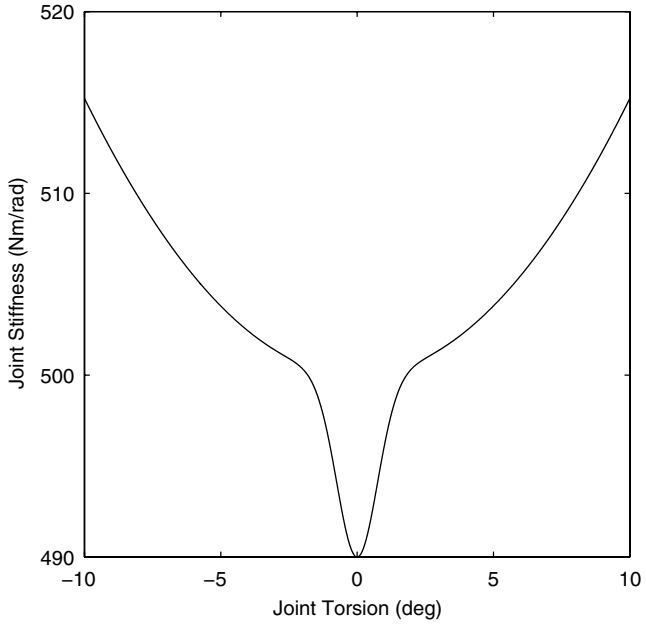

Fig. 4 Nonlinear joint stiffness curve.

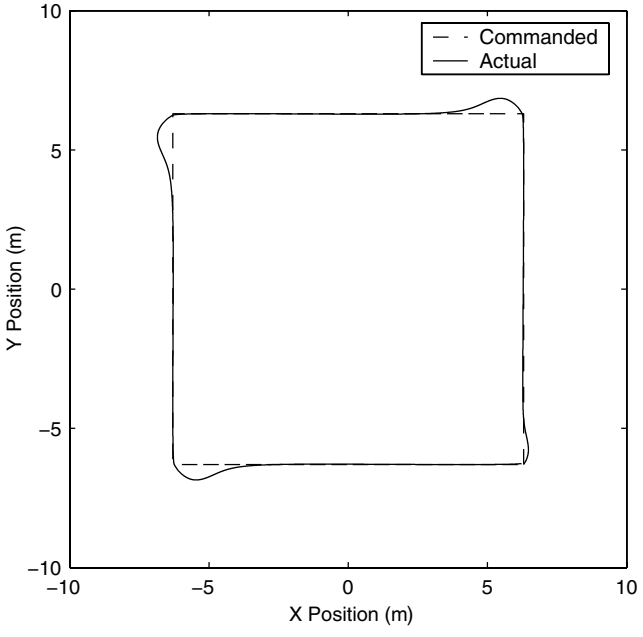

Fig. 6 Nonadaptive control applied to linear joint model.

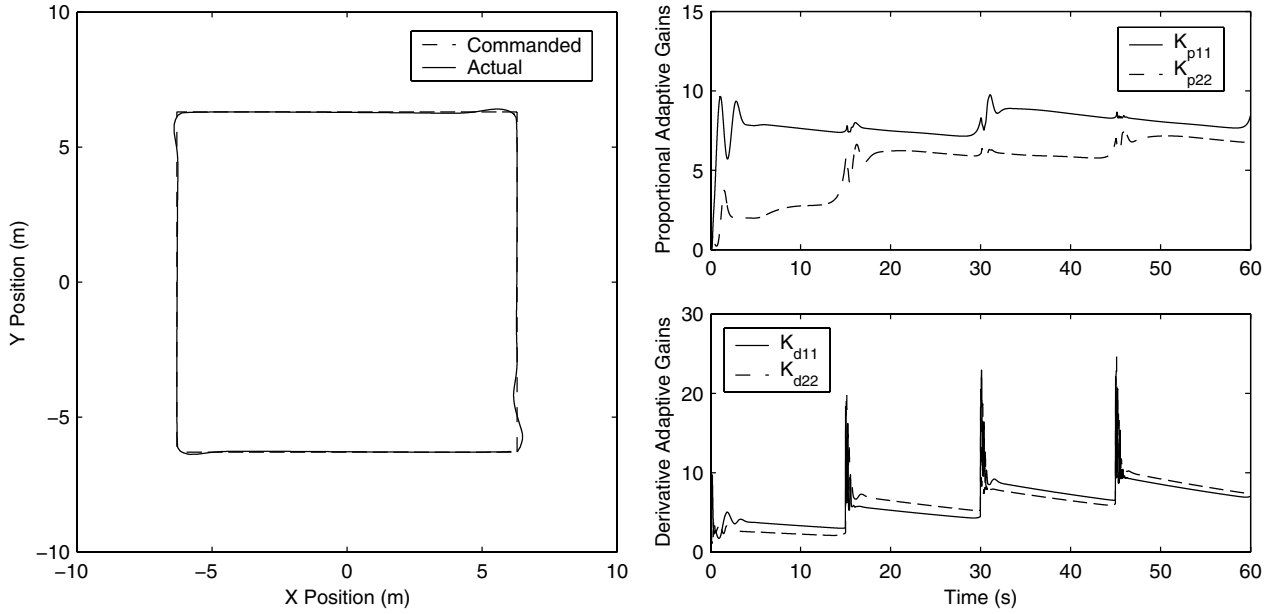

Fig. 7 Adaptive control applied to linear joint model.

The adaptation parameters are chosen as $\Gamma_{pp} = \Gamma_{pi} = 150$ and $\Gamma_{dp} = \Gamma_{di} = 25$, and the gain matrix of the fast-control term is set to $\mathbf{K}_v = \text{diag}[35]\text{N} \cdot \text{m} \cdot \text{s/rad}$. The coefficients σ_p and σ_d have been set to values of 0.008 and 0.023, respectively, which satisfy the condition stated earlier. In fact, these coefficients can be very small, because they are only to prevent the integral adaptive gains from reaching excessively high values or diverging in time. The adaptation algorithm has been activated with $\mathbf{K}_{le}(0) = \mathbf{0}$. These adaptive control gains, parameters and coefficients have been selected to obtain acceptable transient response when applied to the two-link flexible-joint robot modeled with the linear joint dynamics model described earlier: that is, with constant joint stiffness coefficients. For completeness, the adaptive controller is also compared against its nonadaptive version in which the proportional and derivative control gains of the slow control term given by Eq. (39), $\mathbf{K}_p$ and $\mathbf{K}_d$, are kept constant. In an attempt to provide an unbiased comparison between both controllers, the gains of the nonadaptive control law have been selected within the variation range of adaptive control gains obtained in simulations. By doing so, it will be possible to evaluate the benefits of using time-varying gains compared with using constant gains. Based on the adaptation history of the control gains (shown later), the constant gains have been selected as $\mathbf{K}_p = \text{diag}[7]$ and $\mathbf{K}_d = \text{diag}[10]$. For this nonadaptive control strategy, the gain of the fast-control term is set to be the same as for the adaptive controller, i.e., $\mathbf{K}_v = \text{diag}[35]\text{N} \cdot \text{m} \cdot \text{s/rad}$.

Figures 6–15 show the results of end-effector tracking of a 12.6 × 12.6 m square trajectory in 60 s. in a counterclockwise direction starting from rest at the lower-right-hand corner, with the solid lines representing the actual values and the dashed lines representing the commanded, or desired, values. Compared with other type of Cartesian trajectories, such as straight lines or circles, square trajectories represent greater control challenges as each corner of the square represents an abrupt change in directions. Hence, it is required that the end effector reaches each corner and then redirects itself along an orthogonal direction with minimum overshoot and settling time. For this reason, square trajectories are ideal for studying the control of transient vibrations in flexible systems and are commonly used in the literature to assess the trajectory-tracking performance of flexible space manipulators: for example, see [2,3,6,7]. The speed of the commanded square trajectory is fast enough to render the nonlinearities and flexibility effects significant (15 s for each side of the square). As a comparison, a 75 cm square trajectory is tracked in 40 s in [7].

As shown in Fig. 6, when the nonadaptive control strategy is applied to the linear joint stiffness dynamics model, pronounced overshoots of 0.553 m occur at each direction switch, caused by flexibility effects at the joints. However, the trajectory for the adaptive strategy shown in Fig. 7 exhibits minimal overshoots of 0.107, 0.104, and 0.082 m for the first, second, and third direction changes, respectively. Moreover, the adaptive controller settles rapidly to a steady state, such that tracking is close to a straight line along each side of the trajectory. Hence, the response obtained with the adaptive solution is much closer to a square than that of nonadaptive response. The successive increase in tracking performance along each side of the trajectory can be explained by analyzing the adaptation history of the control gains (see Fig. 7). This figure demonstrates that the control gains behave properly; that is, they increase and decrease in accordance with the specific tracking situation, with sudden increases at each direction switch. As explained earlier, the integral term of both adaptive gains is obtained from a first-order filtering of the tracking error. Therefore, once the tracking error begins to decrease as a function of time, the integral terms also decrease, due to the contribution of their respective previous values. The decay in the integral terms occurs at a rate

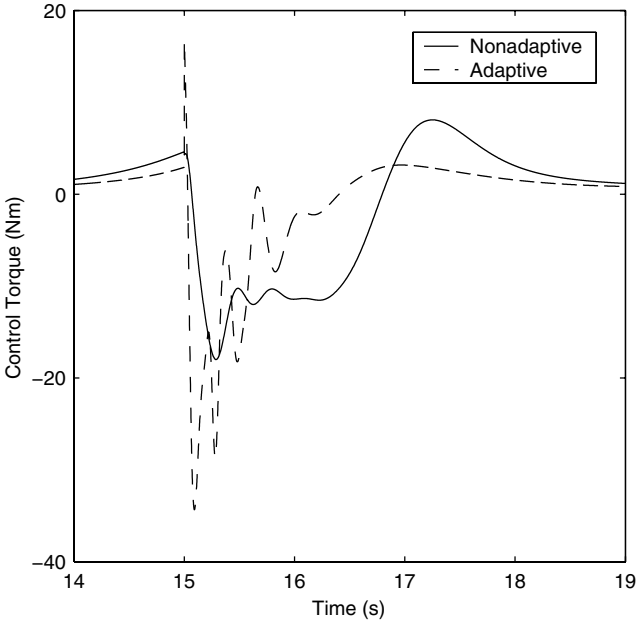

Fig. 8 Joint 1 control torque.

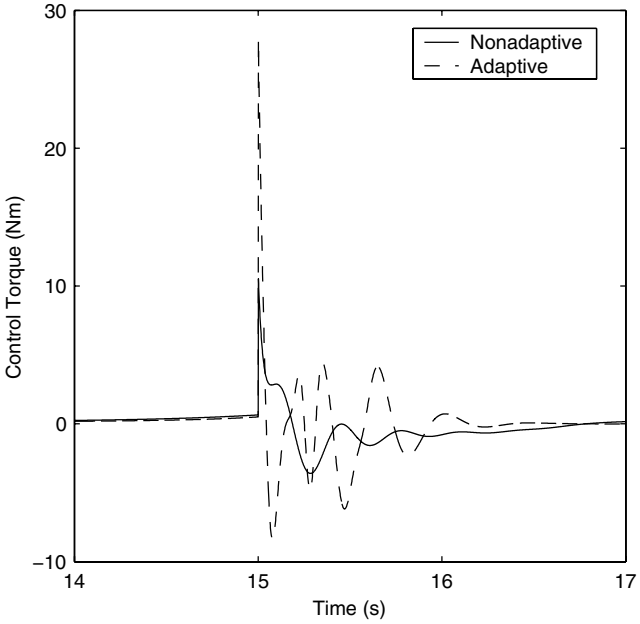

Fig. 9 Joint 2 control torque.

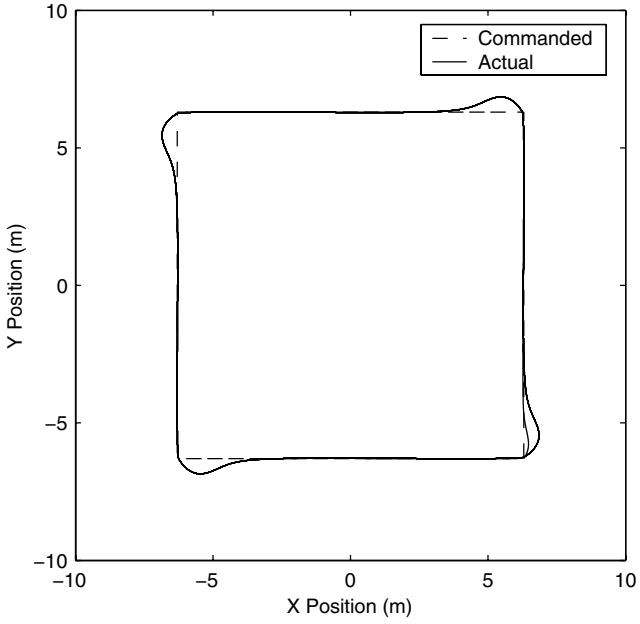

Fig. 10 Nonadaptive control applied to linear joint model: five repetitions.

proportional to σ_p and σ_d. Thus, the greater these two coefficients are, the faster the adaptive gains will decrease between two direction switches. In this particular application, these two coefficients have been selected to be relatively low; hence, the rate of decay of the adaptive gains is also low, and it does not fully compensate for the sudden increase of the adaptive gains at each direction change. This results in slightly higher values of the control gains at each direction change (especially for the derivative control gains) and improvement of the tracking performance at each corner and along each side of the trajectory. It should be noted that for such applications, in which sudden increases in tracking errors occur periodically, it is important that the two coefficients σ_p and σ_d are selected to be greater than zero and in such a way to avoid instability due to excessively high values of the adaptive control gains. As compared with the fixed control gain strategy, these results suggest that a time-varying control gain strategy is better suited to provide good tracking results over a complete trajectory, despite the fact that the fixed gains have been selected within the same range than the adaptive gains, i.e., $\mathbf{K}_p =$ diag[7] and $\mathbf{K}_d =$ diag[10].

It is also important to note that as observed in Fig. 7, the adaptation rates, i.e., the rates of change of the adaptive gains, at each direction switch are relatively large. The high adaptation rates shown in Fig. 7 guarantee that the required gains are provided at the right time, with peaks only at the corners of the square trajectory. Fast adaptation rates allow the controller to use low gains and let them increase only when necessary. As illustrated in Fig. 7, the adaptive gains reached higher peak magnitudes than the constant gain values selected for the nonadaptive control strategy. As a result, the control torque magnitudes and rates associated with the adaptive control strategy are higher than those related to the nonadaptive control scheme, as shown in Figs. 8 and 9. Therefore, when tuning the adaptive controller for use in an actual practical application in which sudden increases in tracking error occur, one has to ensure that the peak magnitudes in adaptive gains do not result in unrealistic control torques that could not be implemented by the joint mechanism hardware selected. In fact, the same consideration must be taken into account when tuning the nonadaptive control. To allow a better

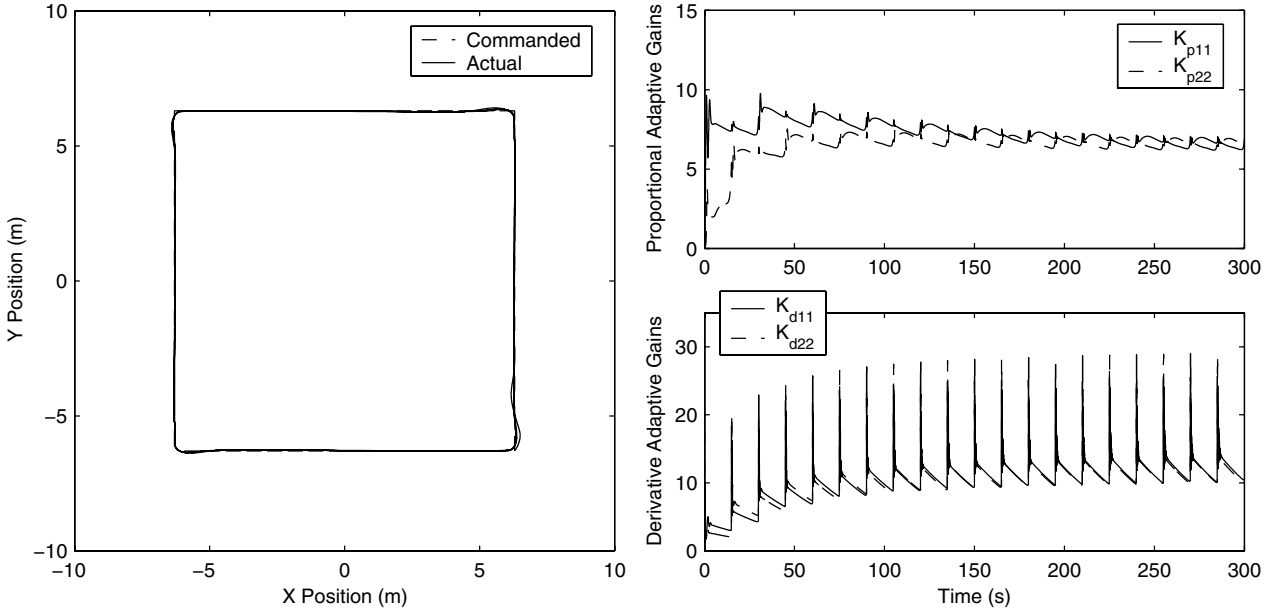

Fig. 11 Adaptive control applied to linear joint model: five repetitions.

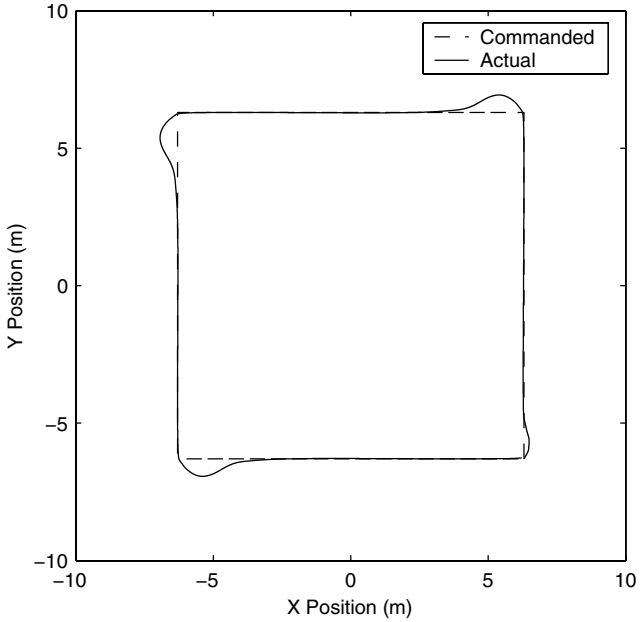

Fig. 12 Nonadaptive control applied to uncertain linear joint model ($\mathbf{k} = \mathbf{diag}[200]\ \mathrm{N \cdot m/rad}$).

tracking performance over the complete trajectory, the fixed gains of the nonadaptive controller would have to be increased to sufficiently high values. Switching direction at high constant gains would, however, be more demanding in terms of required torque amplitudes and torque rates, which could also result in torque rate profiles that could not be handled by typical flexible-joint mechanisms, such as harmonic drives. The maximum control torque peak magnitudes (not shown in the figures) obtained are 52.9 $\mathrm{N \cdot m}$ and 30.24 $\mathrm{N \cdot m}$ for joints 1 and 2 for the nonadaptive controller, compared with 53.3 $\mathrm{N \cdot m}$ and 93.4 $\mathrm{N \cdot m}$ for joints 1 and 2 for the adaptive controller. These peak control efforts occur initially to increase the Cartesian velocity of the end effector along the y-axis from rest to 0.84 $\mathrm{m/s}$. Thereafter, the control torque magnitude reach a maximum levels of 18.0 $\mathrm{N \cdot m}$ and 10.5 $\mathrm{N \cdot m}$ for joints 1 and 2 for the nonadaptive strategy, compared with 43.6 $\mathrm{N \cdot m}$ and 31.8 $\mathrm{N \cdot m}$ at the third direction change for both joints for the adaptive strategy. This means the improved tracking accuracy provided by the adaptive strategy is obtained at the detriment of greater control torque efforts. Still, both nonadaptive and adaptive control torque profiles shown in Figs. 8 and 9 can be implemented by a typical lightweight flexible-joint mechanism (HFUC-2A, Harmonic Drive AG).

For completeness, both the nonadaptive and adaptive composite control strategies have been validated over five consecutive repetitions of the square trajectory (results provided in Figs. 10 and 11). As shown in these figures, both trajectories exhibit stable behaviors over multiple repetitions. The nonadaptive tracking results remain constant at each direction change, with pronounced overshoots of 0.553 m. Meanwhile, compared with the nonadaptive control results, the adaptive strategy exhibits significantly improved tracking results. It must be noted that for the adaptive strategy, the tracking performance is improving during the first two repetitions and remains similar over subsequent repetitions: that is, overshoots at the third direction change of 0.082, 0.066, 0.060, 0.057, and 0.054 m for the first, second, third, fourth and fifth repetitions, respectively. These results are in accordance with the adaptive control gains shown in Fig. 11, whose peak magnitudes are increasing during the first two repetitions, then tend toward constant values during the final three repetitions of the trajectory. This also demonstrates that the tracking errors and adaptive control gains remain bounded over multiple repetitions of the trajectory.

Robustness of the proposed adaptive method to parametric uncertainties can be validated by changing the joint stiffness coefficients of the linear joint stiffness dynamics model. For this reason, a robot equipped with significantly more flexible joints (joint stiffness of $\mathbf{k} = \mathrm{diag}[200]\mathrm{N \cdot m/rad}$) was considered (representing 60% of uncertainty). Using the same control laws as previously (i.e., with control gains tuned with the nominal linear joint stiffness dynamics model $\mathbf{k} = \mathrm{diag}[500]\mathrm{N \cdot m/rad}$), the obtained results are presented in Figs. 12 and 13 for the nonadaptive and the adaptive controllers, respectively. As shown in Fig. 12, the tracking performance of the nonadaptive control strategy is further aggravated and a maximum overshoot of 0.637 m occur at each direction change. The trajectory for the adaptive controller shown in Fig. 13 exhibits overshoots similar to those of the nominal case: that is, 0.095, 0.112, and 0.094 m for the first, second, and third direction changes, respectively. These results illustrate the increased robustness of the adaptive controller and demonstrate that once the adaptive algorithm is properly designed under nominal conditions, the results are not very sensitive to uncertainties in the system parameters. This endorses previous results obtained while validating the MSAC adaptation law under large parametric uncertainties [27].

Similarly, when both controllers are applied to the nonlinear joint stiffness model, the adaptive controller yields smaller overshoots at

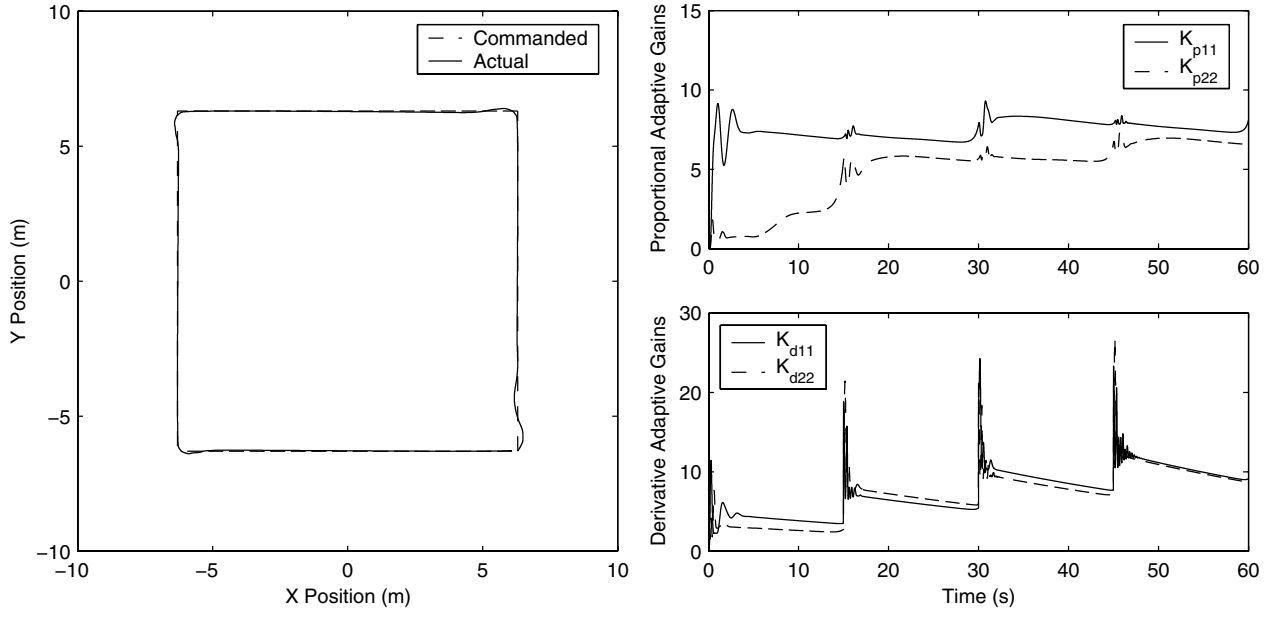

Fig. 13 Adaptive control applied to uncertain linear joint model ($\mathbf{k} = \mathbf{diag}[200]\ \mathrm{N \cdot m/rad}$).

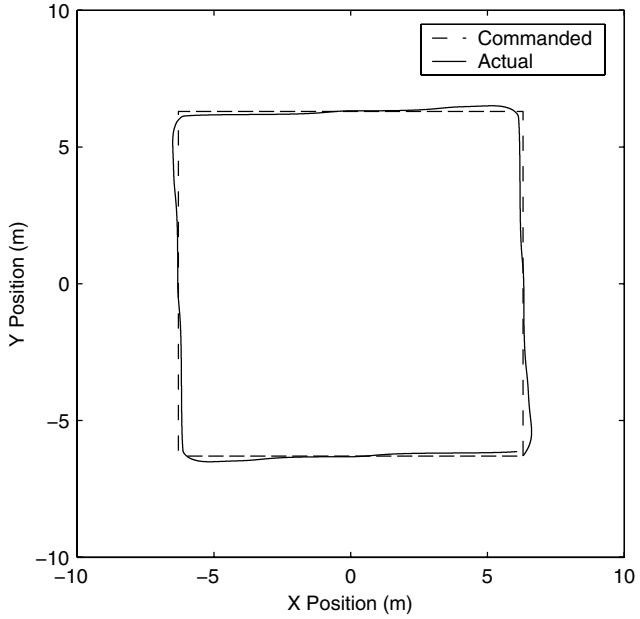

Fig. 14 Nonadaptive control applied to nonlinear joint model.

each direction change, compared with the nonadaptive strategy. This is shown in Figs. 14 and 15, where an overshoot of 0.207 m occurs at each corner of the trajectory for the nonadaptive control strategy, compared with 0.111, 0.092, and 0.081 m for the first, second, and third direction changes for the adaptive controller. Although the nonadaptive control scheme exhibits smaller overshoots than those obtained with the linear joint stiffness model, the end-effector trajectory failed to properly converge to a straight line along each side of the trajectory, as illustrated in Fig. 14. This is due to the nonlinear effects whose introduction in the dynamic model would have required larger gains to stabilize the end effector properly along the square trajectory. Indeed, as shown in Fig. 15 the adaptive gains reached larger magnitudes than previously, as required to minimize the tracking errors. As expected, this suggest that the direct adaptive control scheme copes with modeling errors by adjusting its control gains in order to maintain similar tracking performance than those achieved with the linear joint stiffness model. As mentioned earlier, both controllers were tuned in numerical simulations with the linear joint stiffness model. Hence, these results indicate that the adaptive strategy is more robust to modeling errors, which are due to the introduction of the nonlinear stiffness, soft-windup effect, friction torques, and inertial coupling in the dynamics model.

Finally, the proposed adaptive control law is compared with the well-known Slotine–Li (SLI) indirect adaptive composite controller designed for the same linear joint stiffness model and trajectory-tracking objectives [56]. As demonstrated in [56], the application of the SLI adaptive controller results in similar overshoots (0.078, 0.100, and 0.110 m), but exhibits sustained oscillations that fail to properly converge to a steady-state value along each side of the 12.6×12.6 m benchmark trajectory. Moreover, the SLI adaptive control strategy requires significantly higher control torque magnitudes: 5.0×10^6 N · m and 1.6×10^6 N · m for joints 1 and 2, respectively, which makes it impractical for this specific trajectory-tracking task.

VII. Conclusions

This paper presented the design of a direct adaptive composite controller in which a transpose Jacobian slow control term is added to a fast-control term designed to dampen the elastic vibrations at the joints of a flexible-joint manipulator system. The direct adaptive control system is based on the modified simple adaptive control (MSAC) method, where the errors between the ideal system and the actual system outputs are used to adapt the transpose Jacobian control gains in real time so that tracking errors are reduced. The adaptive controller design was validated in numerical simulations with both the classic linear joint dynamics model and the derived nonlinear joint stiffness model. The proposed nonlinear dynamic formulation for flexible-joint manipulators takes several factors into account that are neglected in most of the existing flexible-joint models: soft-windup, friction, inertial coupling and nonlinear characteristics of joint elasticity. Compared with the nonadaptive transpose Jacobian composite control scheme, the proposed direct adaptive control strategy achieves significantly improved trajectory tracking when applied to both dynamics representations and also proved to be more robust to large uncertainties in the actual joint stiffness coefficients and to modeling errors introduced by the use of the nonlinear joint model. The results are representative of flexible systems, and the MSAC-based direct adaptive control strategy could be extended to a broad range of applications.

Appendix A: Error Dynamics

The differentiation of the state error equation is obtained by subtracting the quasi-steady-state trajectory from the ideal trajectory:

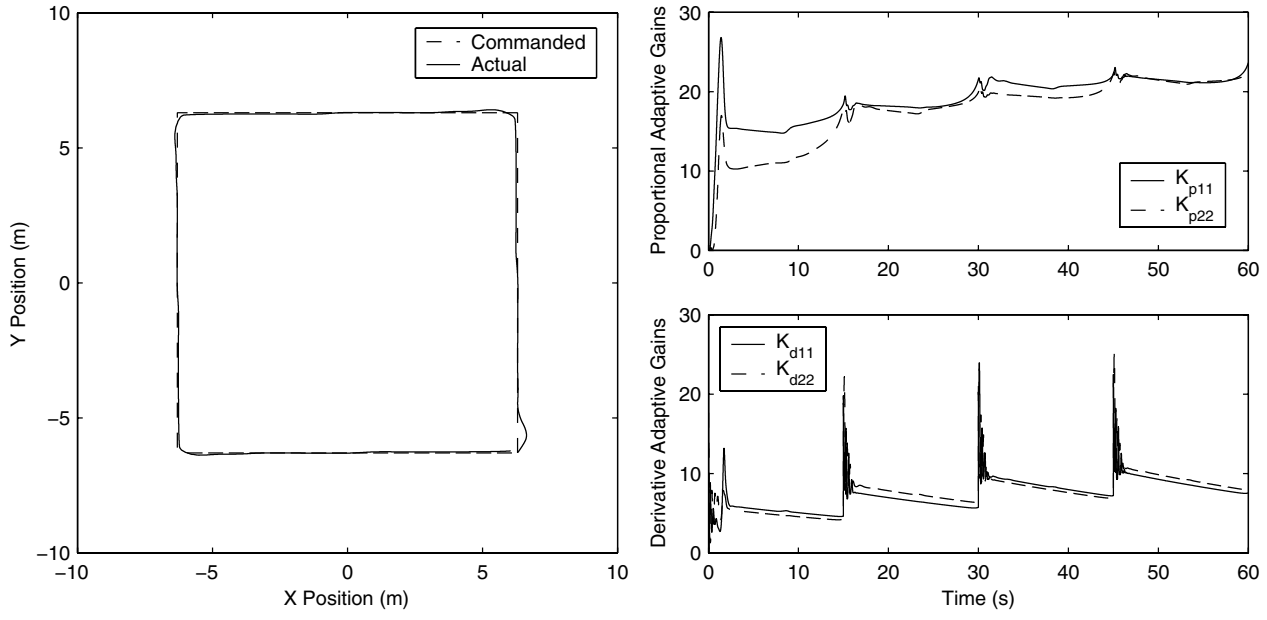

Fig. 15 Adaptive control applied to nonlinear joint model.

$$\dot{\mathbf{e}}_x = \dot{\mathbf{x}}_s^* - \dot{\mathbf{x}}_s = \mathbf{A}_s^*\mathbf{x}_s^* - \mathbf{A}_s\mathbf{x}_s - \mathbf{B}_s\mathbf{K}_e(t)\mathbf{e}_y \tag{A1}$$

Adding and subtracting $\mathbf{A}_s\mathbf{x}_s^*$ to the right side of the equation gives

$$\dot{\mathbf{e}}_x = \mathbf{A}_s^*\mathbf{x}_s^* + (\mathbf{A}_s\mathbf{x}_s^* - \mathbf{A}_s\mathbf{x}_s^*) - \mathbf{A}_s\mathbf{x}_s - \mathbf{B}_s\mathbf{K}_e(t)\mathbf{e}_y \tag{A2}$$

Rearranging yields

$$\dot{\mathbf{e}}_x = \mathbf{A}_s(\mathbf{x}_s^* - \mathbf{x}_s) + (\mathbf{A}_s^* - \mathbf{A}_s)\mathbf{x}_s^* - \mathbf{B}_s\mathbf{K}_e(t)\mathbf{e}_y \tag{A3}$$

Substituting $\mathbf{e}_x$ from Eq. (72),

$$\dot{\mathbf{e}}_x = \mathbf{A}_s\mathbf{e}_x + (\mathbf{A}_s^* - \mathbf{A}_s)\mathbf{x}_s^* - \mathbf{B}_s\mathbf{K}_e(t)\mathbf{e}_y \tag{A4}$$

Adding and subtracting $\mathbf{B}_s\tilde{\mathbf{K}}_e\mathbf{e}_y$ to the right side of the equation gives

$$\dot{\mathbf{e}}_x = \mathbf{A}_s\mathbf{e}_x + (\mathbf{B}_s\tilde{\mathbf{K}}_e\mathbf{e}_y - \mathbf{B}_s\tilde{\mathbf{K}}_e\mathbf{e}_y) + (\mathbf{A}_s^* - \mathbf{A}_s)\mathbf{x}_s^* - \mathbf{B}_s\mathbf{K}_e(t)\mathbf{e}_y \tag{A5}$$

$$\dot{\mathbf{e}}_x = \mathbf{A}_s\mathbf{e}_x - \mathbf{B}_s\tilde{\mathbf{K}}_e\mathbf{e}_y - \mathbf{B}_s(\mathbf{K}_e(t) - \tilde{\mathbf{K}}_e)\mathbf{e}_y + (\mathbf{A}_s^* - \mathbf{A}_s)\mathbf{x}_s^* \tag{A6}$$

Substituting $\mathbf{e}_y$ from Eq. (73) in the second term of the right side of the previous equation gives

$$\dot{\mathbf{e}}_x = (\mathbf{A}_s - \mathbf{B}_s\tilde{\mathbf{K}}_e\mathbf{C}_s)\mathbf{e}_x - \mathbf{B}_s(\mathbf{K}_e(t) - \tilde{\mathbf{K}}_e)\mathbf{e}_y + (\mathbf{A}_s^* - \mathbf{A}_s)\mathbf{x}_s^* \tag{A7}$$

Finally, substituting the adaptive gain $\mathbf{K}_e(t)$ from Eq. (41) yields

$$\dot{\mathbf{e}}_x = (\mathbf{A}_s - \mathbf{B}_s\tilde{\mathbf{K}}_e\mathbf{C}_s)\mathbf{e}_x - \mathbf{B}_s\mathbf{K}_{pe}(t)\mathbf{e}_y - \mathbf{B}_s(\mathbf{K}_{Ie}(t) - \tilde{\mathbf{K}}_e)\mathbf{e}_y + (\mathbf{A}_s^* - \mathbf{A}_s)\mathbf{x}_s^* \tag{A8}$$

Appendix B: Lyapunov Function Derivative

Taking the time derivative of the positive-definite symmetric Lyapunov function (84) gives

$$\dot{V}(\mathbf{e}_x, \mathbf{K}_{Ie}, t) = \dot{\mathbf{e}}_x^T\mathbf{P}\mathbf{e}_x + \mathbf{e}_x^T\dot{\mathbf{P}}\mathbf{e}_x + \mathbf{e}_x^T\mathbf{P}\dot{\mathbf{e}}_x + \operatorname{tr}[\dot{\mathbf{K}}_{Ie}(t)\Gamma_I^{-1}(\mathbf{K}_{Ie}(t) - \tilde{\mathbf{K}}_e)^T] + \operatorname{tr}[(\mathbf{K}_{Ie}(t) - \tilde{\mathbf{K}}_e)\Gamma_I^{-1}\dot{\mathbf{K}}_{Ie}^T(t)^T] \tag{B1}$$

Substituting $\dot{\mathbf{e}}_x$ from Eq. (83) and $\dot{\mathbf{K}}_{Ie}(t)$ from Eq. (77) gives

$$\begin{aligned}\dot{V}(\mathbf{e}_x, \mathbf{K}_{Ie}, t) &= \mathbf{e}_x^T(\mathbf{A}_s - \mathbf{B}_s\tilde{\mathbf{K}}_e\mathbf{C}_s)^T\mathbf{P}\mathbf{e}_x - \mathbf{e}_y^T\mathbf{K}_{pe}^T(t)\mathbf{B}_s^T\mathbf{P}\mathbf{e}_x \\ &\quad - \mathbf{e}_y^T(\mathbf{K}_{Ie}(t) - \tilde{\mathbf{K}}_e)^T\mathbf{B}_s^T\mathbf{P}\mathbf{e}_x + \mathbf{x}_s^{*T}(\mathbf{A}_s^* - \mathbf{A}_s)^T\mathbf{P}\mathbf{e}_x \\ &\quad + \mathbf{e}_x^T\mathbf{P}(\mathbf{A}_s - \mathbf{B}_s\tilde{\mathbf{K}}_e\mathbf{C}_s)\mathbf{e}_x - \mathbf{e}_x^T\mathbf{P}\mathbf{B}_s\mathbf{K}_{pe}(t)\mathbf{e}_y \\ &\quad - \mathbf{e}_x^T\mathbf{P}\mathbf{B}_s(\mathbf{K}_{Ie}(t) - \tilde{\mathbf{K}}_e)\mathbf{e}_y + \mathbf{e}_x^T\mathbf{P}(\mathbf{A}_s^* - \mathbf{A}_s)\mathbf{x}_s^* + \mathbf{e}_x^T\dot{\mathbf{P}}\mathbf{e}_x \\ &\quad + \operatorname{tr}[[\,\mathbf{I}_2 \quad \mathbf{I}_2\,]\operatorname{diag}(\mathbf{e}_y^2)\Gamma_I\Gamma_I^{-1}(\mathbf{K}_{Ie}(t) - \tilde{\mathbf{K}}_e)^T \\ &\quad - \sigma\operatorname{diag}[\mathbf{K}_{Ie}(t)](\mathbf{K}_{Ie}(t) - \tilde{\mathbf{K}}_e)^T] \\ &\quad + \operatorname{tr}\left[(\mathbf{K}_{Ie}(t) - \tilde{\mathbf{K}}_e)\Gamma_I^{-1}\Gamma_I\operatorname{diag}(\mathbf{e}_y^2)\begin{bmatrix}\mathbf{I}_2\\ \mathbf{I}_2\end{bmatrix}\right. \\ &\quad \left. - \sigma(\mathbf{K}_{Ie}(t) - \tilde{\mathbf{K}}_e)\operatorname{diag}[\mathbf{K}_{Ie}(t)]^T\right]\end{aligned} \tag{B2}$$

Substituting $\mathbf{e}_y$ from Eq. (73) and after some algebraic manipulations, one can write

$$\begin{aligned}\dot{V}(\mathbf{e}_x, \mathbf{K}_{Ie}, t) &= \mathbf{e}_x^T(\mathbf{A}_s - \mathbf{B}_s\tilde{\mathbf{K}}_e\mathbf{C}_s)^T\mathbf{P}\mathbf{e}_x - \mathbf{e}_x^T\mathbf{C}_s^T\mathbf{K}_{pe}^T(t)\mathbf{B}_s^T\mathbf{P}\mathbf{e}_x \\ &\quad - \mathbf{e}_x^T\mathbf{C}_s^T(\mathbf{K}_{Ie}(t) - \tilde{\mathbf{K}}_e)^T\mathbf{B}_s^T\mathbf{P}\mathbf{e}_x + \mathbf{x}_s^{*T}(\mathbf{A}_s^* - \mathbf{A}_s)^T\mathbf{P}\mathbf{e}_x \\ &\quad + \mathbf{e}_x^T\mathbf{P}(\mathbf{A}_s - \mathbf{B}_s\tilde{\mathbf{K}}_e\mathbf{C}_s)\mathbf{e}_x - \mathbf{e}_x^T\mathbf{P}\mathbf{B}_s\mathbf{K}_{pe}(t)\mathbf{C}_s\mathbf{e}_x \\ &\quad - \mathbf{e}_x^T\mathbf{P}\mathbf{B}_s(\mathbf{K}_{Ie}(t) - \tilde{\mathbf{K}}_e)\mathbf{C}_s\mathbf{e}_x + \mathbf{e}_x^T\mathbf{P}(\mathbf{A}_s^* - \mathbf{A}_s)\mathbf{x}_s^* + \mathbf{e}_x^T\dot{\mathbf{P}}\mathbf{e}_x \\ &\quad + \operatorname{tr}[[\,\mathbf{I}_2 \quad \mathbf{I}_2\,]\mathbf{C}_s\mathbf{e}_x\mathbf{e}_x^T\mathbf{C}_s^T(\mathbf{K}_{Ie}(t) - \tilde{\mathbf{K}}_e)^T] \\ &\quad + \operatorname{tr}\left[(\mathbf{K}_{Ie}(t) - \tilde{\mathbf{K}}_e)\mathbf{C}_s\mathbf{e}_x\mathbf{e}_x^T\mathbf{C}_s^T\begin{bmatrix}\mathbf{I}_2\\ \mathbf{I}_2\end{bmatrix}\right] \\ &\quad - 2\sigma\operatorname{tr}[\operatorname{diag}[\mathbf{K}_{Ie}(t)](\mathbf{K}_{Ie}(t) - \tilde{\mathbf{K}}_e)^T]\end{aligned} \tag{B3}$$

Because $\operatorname{tr}[AB] = \operatorname{tr}[BA]$,

$$\begin{aligned}\dot{V}(\mathbf{e}_x, \mathbf{K}_{Ie}, t) &= \mathbf{e}_x^T(\mathbf{A}_s - \mathbf{B}_s\tilde{\mathbf{K}}_e\mathbf{C}_s)^T\mathbf{P}\mathbf{e}_x - \mathbf{e}_x^T\mathbf{C}_s^T\mathbf{K}_{pe}^T(t)\mathbf{B}_s^T\mathbf{P}\mathbf{e}_x \\ &\quad - \mathbf{e}_x^T\mathbf{C}_s^T(\mathbf{K}_{Ie}(t) - \tilde{\mathbf{K}}_e)^T\mathbf{B}_s^T\mathbf{P}\mathbf{e}_x + \mathbf{x}_s^{*T}(\mathbf{A}_s^* - \mathbf{A}_s)^T\mathbf{P}\mathbf{e}_x \\ &\quad + \mathbf{e}_x^T\mathbf{P}(\mathbf{A}_s - \mathbf{B}_s\tilde{\mathbf{K}}_e\mathbf{C}_s)\mathbf{e}_x - \mathbf{e}_x^T\mathbf{P}\mathbf{B}_s\mathbf{K}_{pe}(t)\mathbf{C}_s\mathbf{e}_x \\ &\quad - \mathbf{e}_x^T\mathbf{P}\mathbf{B}_s(\mathbf{K}_{Ie}(t) - \tilde{\mathbf{K}}_e)\mathbf{C}_s\mathbf{e}_x + \mathbf{e}_x^T\mathbf{P}(\mathbf{A}_s^* - \mathbf{A}_s)\mathbf{x}_s^* + \mathbf{e}_x^T\dot{\mathbf{P}}\mathbf{e}_x \\ &\quad + \operatorname{tr}[[\,\mathbf{I}_2 \quad \mathbf{I}_2\,]\mathbf{C}_s\mathbf{e}_x\mathbf{e}_x^T\mathbf{C}_s^T(\mathbf{K}_{Ie}(t) - \tilde{\mathbf{K}}_e)^T] \\ &\quad + \operatorname{tr}\left[(\mathbf{K}_{Ie}(t) - \tilde{\mathbf{K}}_e)\mathbf{C}_s\mathbf{e}_x\mathbf{e}_x^T\mathbf{C}_s^T\begin{bmatrix}\mathbf{I}_2\\ \mathbf{I}_2\end{bmatrix}\right] \\ &\quad - 2\sigma\operatorname{tr}[\operatorname{diag}[\mathbf{K}_{Ie}(t)](\mathbf{K}_{Ie}(t) - \tilde{\mathbf{K}}_e)^T]\end{aligned} \tag{B4}$$

Using the ASP conditions (70) and (71) yields

$$\begin{aligned}\dot{V}(\mathbf{e}_x, \mathbf{K}_{Ie}, t) &= -\mathbf{e}_x^T\mathbf{C}_s^T\mathbf{K}_{pe}^T(t)[\,\mathbf{I}_2 \quad \mathbf{I}_2\,]\mathbf{C}_s\mathbf{e}_x - \mathbf{e}_x^T\mathbf{C}_s^T(\mathbf{K}_{Ie}(t) \\ &\quad - \tilde{\mathbf{K}}_e)^T[\,\mathbf{I}_2 \quad \mathbf{I}_2\,]\mathbf{C}_s\mathbf{e}_x + \mathbf{x}_s^{*T}(\mathbf{A}_s^* - \mathbf{A}_s)^T\mathbf{P}\mathbf{e}_x \\ &\quad - \mathbf{e}_x^T\mathbf{C}_s^T\begin{bmatrix}\mathbf{I}_2\\ \mathbf{I}_2\end{bmatrix}\mathbf{K}_{pe}(t)\mathbf{C}_s\mathbf{e}_x - \mathbf{e}_x^T\mathbf{C}_s^T\begin{bmatrix}\mathbf{I}_2\\ \mathbf{I}_2\end{bmatrix}(\mathbf{K}_{Ie}(t) - \tilde{\mathbf{K}}_e)\mathbf{C}_s\mathbf{e}_x \\ &\quad + \mathbf{e}_x^T\mathbf{P}(\mathbf{A}_s^* - \mathbf{A}_s)\mathbf{x}_s^* - \mathbf{e}_x^T\mathbf{Q}\mathbf{e}_x \\ &\quad + \operatorname{tr}[[\,\mathbf{I}_2 \quad \mathbf{I}_2\,]\mathbf{C}_s\mathbf{e}_x\mathbf{e}_x^T\mathbf{C}_s^T(\mathbf{K}_{Ie}(t) - \tilde{\mathbf{K}}_e)^T] \\ &\quad + \operatorname{tr}\left[(\mathbf{K}_{Ie}(t) - \tilde{\mathbf{K}}_e)\mathbf{C}_s\mathbf{e}_x\mathbf{e}_x^T\mathbf{C}_s^T\begin{bmatrix}\mathbf{I}_2\\ \mathbf{I}_2\end{bmatrix}\right] \\ &\quad - 2\sigma\operatorname{tr}[\operatorname{diag}[\mathbf{K}_{Ie}(t)](\mathbf{K}_{Ie}(t) - \tilde{\mathbf{K}}_e)^T]\end{aligned} \tag{B5}$$

Because of the trace properties and the diagonal form of both error and gain matrices, the following equation is obtained:

$$\begin{aligned}\dot{V}(\mathbf{e}_x, \mathbf{K}_{Ie}, t) &= -\mathbf{e}_x^T\mathbf{C}_s^T\mathbf{K}_{pe}^T(t)[\,\mathbf{I}_2 \quad \mathbf{I}_2\,]\mathbf{C}_s\mathbf{e}_x - \mathbf{e}_x^T\mathbf{C}_s^T(\mathbf{K}_{Ie}(t) \\ &\quad - \tilde{\mathbf{K}}_e)^T[\,\mathbf{I}_2 \quad \mathbf{I}_2\,]\mathbf{C}_s\mathbf{e}_x + \mathbf{x}_s^{*T}(\mathbf{A}_s^* - \mathbf{A}_s)^T\mathbf{P}\mathbf{e}_x \\ &\quad - \mathbf{e}_x^T\mathbf{C}_s^T\begin{bmatrix}\mathbf{I}_2\\ \mathbf{I}_2\end{bmatrix}\mathbf{K}_{pe}(t)\mathbf{C}_s\mathbf{e}_x - \mathbf{e}_x^T\mathbf{C}_s^T\begin{bmatrix}\mathbf{I}_2\\ \mathbf{I}_2\end{bmatrix}(\mathbf{K}_{Ie}(t) - \tilde{\mathbf{K}}_e)\mathbf{C}_s\mathbf{e}_x \\ &\quad + \mathbf{e}_x^T\mathbf{P}(\mathbf{A}_s^* - \mathbf{A}_s)\mathbf{x}_s^* - \mathbf{e}_x^T\mathbf{Q}\mathbf{e}_x + \mathbf{e}_x^T\mathbf{C}_s^T(\mathbf{K}_{Ie}(t) \\ &\quad - \tilde{\mathbf{K}}_e)^T[\,\mathbf{I}_2 \quad \mathbf{I}_2\,]\mathbf{C}_s\mathbf{e}_x + \mathbf{e}_x^T\mathbf{C}_s^T\begin{bmatrix}\mathbf{I}_2\\ \mathbf{I}_2\end{bmatrix}(\mathbf{K}_{Ie}(t) - \tilde{\mathbf{K}}_e)\mathbf{C}_s\mathbf{e}_x \\ &\quad - 2\sigma\operatorname{tr}[\operatorname{diag}[\mathbf{K}_{Ie}(t)](\mathbf{K}_{Ie}(t) - \tilde{\mathbf{K}}_e)^T]\end{aligned} \tag{B6}$$

Cancelling equal terms gives

$$\begin{aligned}\dot{V}(\mathbf{e}_x, \mathbf{K}_{Ie}, t) &= -\mathbf{e}_x^T\mathbf{C}_s^T\left(\mathbf{K}_{pe}^T(t)[\,\mathbf{I}_2 \quad \mathbf{I}_2\,] + \begin{bmatrix}\mathbf{I}_2\\ \mathbf{I}_2\end{bmatrix}\mathbf{K}_{pe}(t)\right)\mathbf{C}_s\mathbf{e}_x \\ &\quad + 2\mathbf{e}_x^T\mathbf{P}(\mathbf{A}_s^* - \mathbf{A}_s)\mathbf{x}_s^* - \mathbf{e}_x^T\mathbf{Q}\mathbf{e}_x - 2\sigma\operatorname{tr}[\operatorname{diag}[\mathbf{K}_{Ie}(t)](\mathbf{K}_{Ie}(t) \\ &\quad - \tilde{\mathbf{K}}_e)^T]\end{aligned} \tag{B7}$$

Finally, adding and subtracting $2\sigma\,\mathrm{tr}[\tilde{\mathbf{K}}_e(\mathbf{K}_{Ie}(t)-\tilde{\mathbf{K}}_e)^T]$ to the last term gives

$$\dot{V}(\mathbf{e}_x,\mathbf{K}_{Ie},t)=-\mathbf{e}_x^T\mathbf{Q}\mathbf{e}_x-2\sigma\,\mathrm{tr}[(\mathbf{K}_{Ie}(t)-\tilde{\mathbf{K}}_e)(\mathbf{K}_{Ie}(t)-\tilde{\mathbf{K}}_e)^T]$$
$$-\mathbf{e}_y^T\left(\mathbf{K}_{pe}(t)[\,\mathbf{I}_2\quad\mathbf{I}_2\,]+\begin{bmatrix}\mathbf{I}_2\\ \mathbf{I}_2\end{bmatrix}\mathbf{K}_{pe}(t)\right)\mathbf{e}_y+2\mathbf{e}_x^T\mathbf{P}(\mathbf{A}_s^*-\mathbf{A}_s)\mathbf{x}_s^*$$
$$-2\sigma\,\mathrm{tr}[\tilde{\mathbf{K}}_e(\mathbf{K}_{Ie}(t)-\tilde{\mathbf{K}}_e)^T] \tag{B8}$$

Acknowledgments

This research was financially supported in part by the Canadian Space Agency, the Canadian Armed Forces under the Honorary Colonel S. B. Lerner Memorial Educational Bursary, and the Natural Sciences and Engineering Research Council of Canada under the Alexander Graham Bell Canada Graduate Scholarship CGS D3-374291-2009.

References

[1] Sasiadek, J. Z., and Srinivasan, R., "Dynamic Modeling and Adaptive Control of a Single-Link Flexible Manipulator," *Journal of Guidance, Control, and Dynamics*, Vol. 12, No. 6, 1989, pp. 838–844. doi:10.2514/3.20489

[2] Green, A., and Sasiadek, J. Z., "Adaptive Control of a Flexible Robot Using Fuzzy Logic," *Journal of Guidance, Control, and Dynamics*, Vol. 28, No. 1, 2005, pp. 36–42. doi:10.2514/1.6376

[3] Banerjee, A. K., and Singhose, W., "Command Shaping in Tracking Control of a Two-Link Flexible Robot," *Journal of Guidance, Control, and Dynamics*, Vol. 21, No. 6, 1998, pp. 1012–1015. doi:10.2514/2.4343

[4] Hecht, N. K., and Junkins, J. L., "Near-Minimum-Time Control of a Flexible Manipulator," *Journal of Guidance, Control, and Dynamics*, Vol. 15, No. 2, 1992, pp. 477–481. doi:10.2514/3.20860

[5] De Luca, A., and Siciliano, B., "Inversion-Based Nonlinear Control of Robot Arms with Flexible Links," *Journal of Guidance, Control, and Dynamics*, Vol. 16, No. 6, 1993, pp. 1169–1176. doi:10.2514/3.21142

[6] Romano, M., Agrawal, B. N., and Bernelli-Zazerra, F., "Experiments on Command Shaping Control of a Manipulator with Flexible Links," *Journal of Guidance, Control, and Dynamics*, Vol. 25, No. 2, 2002, pp. 232–239. doi:10.2514/2.4903

[7] Carusone, J., Buchan, K. S., and D'Eleuterio, G. M. T., "Experiments in End-Effector Tracking Control for Structurally Flexible Space Manipulators," *IEEE Transactions on Robotics and Automation*, Vol. 9, No. 5, 1993, pp. 553–560. doi:10.1109/70.258048

[8] Damaren, C. J., "Modal Properties and Control System Design for Two-Link Flexible Manipulators," *International Journal of Robotics Research*, Vol. 17, No. 6, 1998, pp. 667–678. doi:10.1177/027836499801700606

[9] Sweet, L. M., and Good, M. C., "Re-Definition of the Robot Motion Control Problem: Effects of Plant Dynamics, Drive System Constraints, and User Requirements," *23rd IEEE Conference on Decision and Control*, Inst. of Electrical and Electronics Engineers, Piscataway, NJ, Dec. 1984, pp. 724–732.

[10] van Woerkoma, P. T. L. M., and Misrab, A. K., "Robotic Manipulators in Space: A Dynamics and Control Perspective," *Acta Astronautica*, Vol. 38, Nos. 4–8, 1996, pp. 411–421. doi:10.1016/0094-5765(96)00018-5

[11] Chen, Y., Jin, J., Wu, X., et al. "Analysis of Dynamical Behavior of a Planetary Gear Train," *Intelligent Robotics and Applications, Lecture Notes in Computer Science*, Springer, Berlin, 2008, pp. 46–53.doi: 10.1007/978-3-540-88513-9_6

[12] Kahraman, A., and Vijayakar, S., "Effect of Internal Gear Flexibility on the Quasi-Static Behavior of a Planetary Gear Set," *Journal of Mechanical Design*, Vol. 123, No. 3, 2001, pp. 408–415. doi:10.1115/1.1371477

[13] Reintsema, D., Landzettel, K., Hirzinger, G., et al., "DLR's Advanced Telerobotic Concepts and Experiments for On-Orbit Servicing," *Advances in Telerobotics*, edited by M. Ferre, et al., Springer–Verlag, Berlin, 2007, pp. 323–345.

[14] Sasiadek, J. Z., "Space Robotics and Manipulators—The Past and the Future," *Control Engineering Practice*, Vol. 2, No. 3, 1994, pp. 491–497. doi:10.1016/0967-0661(94)90787-0

[15] Spong, M. W., Khorasani, K., and Kokotovic, P. V., "An Integral Manifold Approach to the Feedback Control of Flexible Joint Robots," *IEEE Journal of robotics and automation*, Vol. 3, No. 4, 1987, pp. 291–300. doi:10.1109/JRA.1987.1087102

[16] Cetinkunt, S., and Book, W. J., "Flexibility Effects on the Control System Performance of Large Scale Robotic Manipulators," *Journal of the Astronautical Sciences*, Vol. 38, No. 4, 1990, pp. 531–556.

[17] Ghorbel, F., Hung, J. Y., and Spong, M. W., "Adaptive Control of Flexible Joint Manipulators," *IEEE Control Systems Magazine*, Vol. 9, No. 7, 1989, pp. 9–13. doi:10.1109/37.41450

[18] Sasiadek, J. Z., "Space Robotics and Manipulators: Lessons Learned from the Past and Future Missions and Systems," *12th International IFAC Symposium on Automatic Control in Aerospace*, Ottobrunn, Germany, Sept. 1992.

[19] Khalil, H. K., *Nonlinear Systems*, Macmillan, New York, 1992, pp. 437–484.

[20] Spong, M. W., "Adaptive Control of Flexible Joint Manipulators," *Systems and Control Letters*, Vol. 13, 1989, pp. 15–21. doi:10.1016/0167-6911(89)90016-9

[21] Spong, M. W., "Adaptive Control of Flexible Joint Manipulators: Comments on Two Papers," *Automatica*, Vol. 31, No. 4, 1995, pp. 585–590. doi:10.1016/0005-1098(95)98487-Q

[22] Chang, Y. Z., and Daniel, R. W., "On the Adaptive Control of Flexible Joint Robots," *Automatica*, Vol. 28, No. 5, 1992, pp. 969–974. doi:10.1016/0005-1098(92)90149-A

[23] Ott, C., Albu-Schaffer, A., and Hirzinger, G., "Comparison of Adaptive and Nonadaptive Tracking Control Laws for a Flexible Joint Manipulator," *IEEE International Conference on Intelligent Robots and Systems*, Inst. of Electrical and Electronics Engineers, Piscataway, NJ, Oct. 2002, pp. 2018–2024.

[24] Huang, L., Ge, S. S., and Lee, T. H., "Position/Force Control of Uncertain Constrained Flexible Joint Robots," *Mechatronics*, Vol. 16, No. 2, 2006, pp. 111–120. doi:10.1016/j.mechatronics.2005.10.002

[25] Subudhi, B., and Morris, A. S., "Singular Perturbation Approach to Trajectory Tracking of Flexible Robot with Joint Elasticity," *International Journal of Systems Science*, Vol. 34, No. 3, 2003, pp. 167–179. doi:10.1080/0020772031000135450

[26] Cao, Y., and de Silva, C. W., "Dynamic Modeling and Neural-Network Adaptive Control of a Deployable Manipulator System," *Journal of Guidance, Control, and Dynamics*, Vol. 29, No. 1, 2006, pp. 192–194. doi:10.2514/1.11032

[27] Ulrich, S., and de Lafontaine, J., "Autonomous Atmospheric Entry on Mars: Performance Improvement Using a Novel Adaptive Control Algorithm," *Journal of the Astronautical Sciences*, Vol. 55, No. 4, 2007, pp. 431–449.

[28] Kaufman, H., Barkana, I., and Sobel, K., *Direct Adaptive Control Algorithms: Theory and Applications*, 2nd ed., Communications and Control Engineering Series, Springer, New York, 1997, pp. 53–59, 241–292, 326–330.

[29] Spong, M. W., "Modeling and Control of Elastic Joint Robots," *Journal of Dynamic Systems, Measurement, and Control*, Vol. 109, No. 4, 1987, pp. 310–319. doi:10.1115/1.3143860

[30] Kircanski, N. M., and Goldenberg, A. A., "An Experimental Study of Nonlinear Stiffness, Hysteresis, and Friction Effects in Robot Joints with Harmonic Drives and Torque Sensors," *International Journal of Robotics Research*, Vol. 16, No. 2, 1997, pp. 214–239. doi:10.1177/027836499701600207

[31] Hidaka, T., Ishida, T., Zhang, Y., Sasahara, M., and Tanioka, Y., "Vibration of a Strain-Wave Gearing in an Industrial Robot," *ASME International Power Transmission and Gearing Conference*, 1990, pp. 789–794.

[32] Tuttle, T. D., and Seering, W. P., "A Nonlinear Model of a Harmonic Drive Gear Transmission," *IEEE Transactions on Robotics and Automation*, Vol. 12, No. 3, 1996, pp. 368–374. doi:10.1109/70.499819

[33] Taghirad, H. D., and Bélanger, P. R., "Modeling and Parameter Identification of Harmonic Drive Systems," *Journal of Dynamic Systems, Measurement, and Control*, Vol. 120, No. 4, 1998, pp. 439–444.

doi:10.1115/1.2801484
[34] Li, Z., Melek, W. W., and Clark, C., "Decentralized Robust Control of Robot Manipulators with Harmonic Drive Transmission and Application to Modular and Reconfigurable Serial Arms," *Robotica*, Vol. 27, 2009, pp. 291–302. doi:10.1017/S0263574708004712
[35] Lozano, R., Valera, A., Albertos, P., Arimoto, S., and Nakayama, T., "PD Control of Robot Manipulators with Joint Flexibility, Actuators Dynamics and Friction," *Automatica*, Vol. 35, No. 10, 1999, pp. 1697–1700. doi:10.1016/S0005-1098(99)00083-7
[36] Spong, M. W., Hutchinson, S., and Vidyasagar, M., *Robot Modeling and Control*, Wiley, New York, 2006, pp. 85; 134; 240–250; 259–262.
[37] De Wit, C., Noel, P., Aubin, A., and Brogliato, B., "Adaptive Friction Compensation in Robot Manipulators: Low Velocities," *International Journal of Robotics Research*, Vol. 10, No. 3, 1991, pp. 189–199. doi:10.1177/027836499101000301
[38] Makkar, C., Dixon, W. E., Sawyer, W. G., and Hu, G., "A New Continuously Differentiable Friction Model for Control Systems Design," *2005 IEEE/ASME International Conference on Advanced Intelligent Mechatronics*, Inst. of Electrical and Electronics Engineers, Piscataway, NJ, July 2005, pp. 600–605.
[39] Lightcap, C. A., "Measurement and Control Issues in a Novel Dynamic Radiographic Imaging System," Ph.D. Thesis, University of Florida, Gainesville, FL, 2008.
[40] Lightcap, C. A., and Banks, S. A., "An Extended Kalman Filter for Real-Time Estimation and Control of a Rigid-Link Flexible-Joint Manipulator," *IEEE Transactions on Control Systems Technology*, Vol. 18, No. 1, 2010, pp. 91–103. doi:10.1109/TCST.2009.2014959
[41] ElMaraghy, H. A., Lahdhiri, T., and Ciuca, F., "Robust Linear Control of Flexible Joint Robot Systems," *Journal of Intelligent and Robotic Systems: Theory and Applications*, Vol. 34, No. 4, 2002, pp. 335–356. doi:10.1023/A:1019683316155
[42] Moghaddam, M. M., and Goldenberg, A. A., "Nonlinear Modeling and Robust $\mathcal{H}_\infty$-Based Control of Flexible Joint Robots with Harmonic Drives," *Proceedings of the IEEE International Conference on Robotics and Automation*, Inst. of Electrical and Electronics Engineers, Piscataway, NJ, April 1997, pp. 3130–3135.
[43] Barkana, I., "Classical and Simple Adaptive Control for Nonminimum Phase Autopilot Design," *Journal of Guidance, Control, and Dynamics*, Vol. 28, No. 4, 2005, pp. 631–638. doi:10.2514/1.9542
[44] Sobel, K., Kaufman, H., and Mabius, L., "Implicit Adaptive Control for a Class of MIMO Systems," *IEEE Transactions on Aerospace and Electronic Systems*, Vol. 18, No. 5, 1982, pp. 576–589. doi:10.1109/TAES.1982.309270
[45] Barkana, I., Kaufman, H., and Balas, M., "Model Reference Adaptive Control of Large Structural Systems," *Journal of Guidance, Control, and Dynamics*, Vol. 6, No. 2, 1983, pp. 112–118. doi:10.2514/3.8544
[46] Barkana, I., and Kaufman, H., "Some Applications of Direct Adaptive Control to Large Structural Systems," *Journal of Guidance, Control, and Dynamics*, Vol. 7, No. 6, 1984, pp. 717–724. doi:10.2514/3.19918
[47] Barkana, I., and Kaufman, H., "Global Stability and Performance of a Simplified Adaptive Algorithm," *International Journal of Control*, Vol. 42, No. 6, 1985, pp. 1419–1505. doi:10.1080/00207178508933440
[48] Morse, W. D., and Ossman, K. A., "Model Following Reconfigurable Flight Control System for the AFTI/F-16," *Journal of Guidance, Control, and Dynamics*, Vol. 13, No. 6, 1990, pp. 969–976. doi:10.2514/3.20568
[49] Mooij, E., "Numerical Investigation of Model Reference Adaptive Control for Hypersonic Aircraft," *Journal of Guidance, Control, and Dynamics*, Vol. 24, No. 2, 2001, pp. 315–323. doi:10.2514/2.4714
[50] Ulrich, S., and de Lafontaine, J., "Development of a Novel Adaptive Control Algorithm for a Fighter Aircraft," AIAA Guidance, Navigation and Control Conference and Exhibit, Hilton Head, SC, AIAA Paper 2007-6649, Aug. 2007.
[51] Naidu, D. S., and Calise, A. J., "Singular Perturbations and Time Scales in Guidance and Control of Aerospace Systems: A Survey," *Journal of Guidance, Control, and Dynamics*, Vol. 24, No. 6, 2001, pp. 1057–1078. doi:10.2514/2.4830
[52] Craig, J. J., *Introduction to Robotics: Mechanics and Control*, 3rd ed., Prentice–Hall, Upper Saddle River, NJ, 2005, pp. 307–311.
[53] Ioannou, P. A., and Kokotovik, P. V., "Singular Perturbation and Robust Redesign of Adaptive Control," *21st IEEE Decision and Control Conference*, Inst. of Electrical and Electronics Engineers, Piscataway, NJ, 1982, pp. 24–29.
[54] Barkana, I., "Output Feedback Stabilizability and Passivity in Nonstationary and Nonlinear Systems," *International Journal of Adaptive Control and Signal Processing*, Vol. 24, No. 7, 2010, pp. 568–591. doi:10.1002/acs.1149
[55] Chung, W., Fu, L.-C., and Hsu, S.-H., "Motion Control," *Springer Handbook of Robotics*, edited by B. Siciliano, and O. Khatib, Springer–Verlag, Berlin, 2008, pp. 133–159.
[56] Ulrich, S., and Sasiadek, J. Z., "Control Strategies for Flexible Joint Manipulators," AIAA Guidance, Navigation, and Control Conference, Portland, OR, AIAA Paper 2011-6297, Aug. 2011.